BBA - Molecular Basis of Disease 1865 (2019) 1361–1378

Contents lists available at ScienceDirect

BBA - Molecular Basis of Disease

journal homepage: www.elsevier.com/locate/bbadis

Two mechanisms involving the autophagic and proteasomal pathways process the metastasis suppressor protein, N-myc downstream regulated gene 1

Sumit Sahni[a,*,1], Kyung Chan Park[a], Zaklina Kovacevic[a], Des R. Richardson[a,b,*,1]

[a] Molecular Pharmacology and Pathology Program, Department of Pathology and Bosch Institute, Medical Foundation Building (K25), University of Sydney, Sydney, New South Wales 2006, Australia

[b] Department of Pathology and Biological Responses, Nagoya University Graduate School of Medicine, Nagoya 466-8550, Japan

ARTICLE INFO

Keywords:
NDRG1
Autophagy
Proteasome
Metastatic suppressor

ABSTRACT

N-myc downstream regulated gene 1 (NDRG1) is an intriguing metastasis suppressor protein, which plays an important role in suppressing multiple oncogenic signaling pathways. Interestingly, multiple isoforms of NDRG1 have been identified, although the molecular mechanisms involved in their generation remains elusive. Herein, we demonstrate the role of two mechanisms involving autophagic and proteasomal machinery as part of an intricate system to generate different NDRG1 isoforms. Examining multiple pancreatic cancer cell-types using immunoblotting demonstrated three major isoforms of NDRG1 at approximately 41-, 46- and 47-kDa. The top NDRG1 band at 47-kDa was shown to be processed by the proteasome, followed by autophagic metabolism of the middle NDRG1 band at 46-kDa. The role of the proteasomal and autophagic pathways in NDRG1 processing was further confirmed by co-localization analysis of confocal images using PSMD9 and LC3 as classical markers of these respective pathways. All NDRG1 isoforms were demonstrated to be, at least in part, phosphorylated forms of the protein. Inhibition of two well-characterized upstream kinases of NDRG1, namely GSK3β and SGK1, resulted in decreased levels of the top NDRG1 band. Studies demonstrated that inhibition of GSK3β decreased levels of the top 47-kDa NDRG1 band, independent of its kinase activity, and this effect was not mediated *via* the proteasomal pathway. In contrast, the decrease in the top NDRG1 band at 47-kDa after SGK1 inhibition, was due to suppression of its kinase activity. Overall, these studies elucidated the complex and intricate regulatory pathways involving both proteasomal and autophagic processing of the metastasis suppressor protein, NDRG1.

1. Introduction

N-myc downstream regulated gene 1 (NDRG1) is a potent metastasis suppressor, which inhibits multiple oncogenic signaling pathways in various cancers [1,2]. Indeed, its anti-oncogenic functions have been demonstrated *in vitro* [3–5] and *in vivo* [6,7], making this protein an important therapeutic target for development of novel anti-cancer therapies. While the molecular functions of NDRG1 have been elucidated in various cancers [2], including its role as a broad inhibitor of oncogenic signaling [3,4,8–10], the exact mechanism(s) involved in its cellular processing and degradation remain elusive.

The *NDRG1* gene, which is located on chromosome 8q24.3 [11], encodes a 3.0-kb mRNA that translates to a protein comprised of 394 amino acids [12,13]. NDRG1 is a member of the NDRG family, which consists of four family members, NDRG1–4 [14]. Unlike other NDRG members, NDRG1 has a three tandem (GTRSRSHTSE) repeat sequences near its *C*-terminus end [14]. Assessment of NDRG1 protein expression by immunoblotting revealed the existence of multiple isoforms of the protein in six different tumor cell-types, with two major bands at ~41- and ~46-kDa and a faint third band that was differentially expressed between the cell-types at ~47-kDa [15].

The multiple NDRG1 bands observed in immunoblots are probably

Abbreviations: Baf A1, Bafilomycin A1; Dp44mT, di-2-pyridylketone 4,4-dimethyl-3-thiosemicarbazone; GSK3β, glycogen synthase kinase 3β; GSKI, GSK3β-inhibitor SB216763; HIF-1α, hypoxia inducible factor-1α; NDRG1, N-myc downstream regulated gene 1; SGK1, serum- and glucocorticoid-regulated kinase 1; SGKI, SGK1-inhibitor; SUMO, small ubiquitin-like modifier; 3-MA, 3-methyladenine

* Corresponding authors at: Molecular Pharmacology and Pathology Program, Department of Pathology and Bosch Institute, University of Sydney, Sydney, New South Wales 2006, Australia.

E-mail addresses: sumit.sahni@sydney.edu.au (S. Sahni), d.richardson@usyd.med.edu.au (D.R. Richardson).

[1] Contributed equally to the work as co-corresponding and senior authors.

https://doi.org/10.1016/j.bbadis.2019.02.008
Received 29 November 2018; Received in revised form 25 January 2019; Accepted 8 February 2019
Available online 11 February 2019
0925-4439/

the result of post-translational modifications such as phosphorylation [16], small ubiquitin-like modifier (SUMO) modification [17] and/or cleavage of NDRG1 [18]. Proteasome-mediated NDRG1 degradation was previously reported and NDRG1 phosphorylation was suggested to signal this degradation pathway [19,20]. Phosphorylation of NDRG1 at Ser330 and Thr346 by serum- and glucocorticoid-regulated kinase 1 (SGK1) was shown to be crucial to inhibit NF-κB signaling and CXC cytokine synthesis [21]. Additionally, NDRG1 cleavage was identified in prostate cancer cells, but not normal prostate epithelial cells, suggesting this process could influence the anti-oncogenic function of NDRG1 [18].

Our previous studies have demonstrated that NDRG1 is up-regulated by cellular iron depletion and hypoxia through hypoxia-inducible factor-1α (HIF-1α)-dependent and -independent mechanisms at protein and mRNA levels [22–24]. Furthermore, due to its well-characterized roles as a metastasis suppressor, and since metastasis kills 90% of cancer patients [25], NDRG1 has been identified as a molecular target of a new group of anti-cancer agents of the di-2-pyridylketone thiosemicarbazone class that potently inhibit tumor growth and metastasis [6,22,26–32]. The first lead agent of this class of agents, di-2-pyridylketone 4,4-dimethyl-3-thiosemicarbazone (Dp44mT), leads to marked NDRG1 up-regulation in many tumor cell-types [15,22,28,33], with an analogue of this agent entering Phase I clinical trials [34]. In fact, relative to control-treated cells, Dp44mT induced up-regulation of the 46- and 47-kDa NDRG1 bands, as well as increasing the p-NDRG1 (Ser330 and Thr346) bands at 46–47-kDa [15].

Herein, we demonstrate that there was a significant increase in the top 47-kDa NDRG1 band by two well-characterized proteasomal inhibitors. In contrast, the autophagic inhibitor, Baf A1, increased levels of the middle 46-kDa NDRG1 band. Sequential processing of NDRG1 was evident as simultaneous inhibition of the proteasomal and autophagic pathways resulted in only the top 47-kDa band, with no alteration in the middle 46-kDa band. All three NDRG1 isoforms were, at least in part, phosphorylated at Ser330 and Thr346. The top NDRG1 band in immunoblots was suppressed by the inhibition of well-characterized upstream kinases of NDRG1, namely glycogen synthase kinase 3β (GSK3β) and SGK1. Notably, GSK3β inhibition was demonstrated to be involved in a kinase-independent decrease in NDRG1 that may be related to up-regulation of a lysosomal processing. On the other hand, SGK1 inhibition, was mediated through its ability to inhibit NDRG1 phosphorylation. Taken together, these studies indicate complex processing of NDRG1 in pancreatic cancer cells.

2. Materials and methods

2.1. Cell culture

PANC1, CFPAC-1 and AsPC-1 human pancreatic cancer cell lines were purchased from the American Type Culture Collection (ATCC, Manassas, VA). Cell lines were authenticated by the provider and this was based on viability, recovery, growth, morphology, cytogenetic analysis, antigen expression, DNA profile and isoenzymology. Cells were routinely examined for mycoplasma contamination using standard methods [35]. Cells were grown in Dulbecco's modified Eagle's medium (DMEM) or RPMI medium supplemented with 10% fetal bovine serum (FBS), 1% (v/v) non-essential amino acids, 1% sodium pyruvate, and 1% penicillin/streptomycin/glutamine (Sigma-Aldrich, St. Louis, MO). The cells were grown at 37 °C in an atmosphere of 95% air and 5% CO_2.

2.2. Chemicals and treatments

The chelator, Dp44mT, was synthesized and characterized, as described previously [36]. The inhibitors, 3-methyladenine (3-MA), MG132, Bafilomycin A1, Expoxomycin, E64D, SB216763, LiCl and GSK650394 were purchased from Sigma-Aldrich. Cells were seeded into tissue culture plates and incubated until approximately 80% confluence. These cells were then treated with different inhibitors, alone or with Dp44mT, at the indicated concentrations for 24 h/37 °C, unless otherwise specified. In order to minimise any cellular toxicity, inhibitors were used at previously established doses for pancreatic cancer cells that were optimised by preliminary experiments, *i.e.*, MG132 (0.5–10 μM; [37]); Baf A1 (5–100 nM; [38,39]), 3-MA (0.25–4 mM; [40]) and Dp44mT (10 μM; [4]).

2.3. Protein extraction and immunoblotting

Protein extraction and immunoblot analysis was performed by standard methods [41]. The primary antibodies used included those against: NDRG1 (Cat. # ab37897; Abcam Inc., Cambridge, UK), pSer330-NDRG1 (Cat. # 3506; Cell Signaling Technology; Danvers, MA), pThr346-NDRG1 (Cat. # 3217; Cell Signaling Technology) and HIF-1α (Cat# 610959; BD Transduction Labs, San Jose, CA). The phospho-NDRG1 antibodies used in this study are very well characterized and widely used in the literature for detecting p-NDRG1 levels [28,42–44]. Indeed, the manufacturer has performed the studies using lambda phosphatase, which completely abrogates the antibody signal.

The primary antibodies were diluted 1:1000 in 5% (w/v) bovine serum albumin (BSA) in Tris-buffered saline (TBS; Sigma-Aldrich) containing 0.1% Tween-20 (TBST) or 5% non-fat milk in TBST. The secondary antibodies used were horseradish peroxide (HRP)-conjugated anti-goat (Cat. # A5420; Sigma-Aldrich), anti-rabbit (Cat. # A6154; Sigma-Aldrich) and anti-mouse (Cat. # A4416; Sigma-Aldrich).

As an assessment of equal protein-loading, membranes were probed for β-actin (Cat #A1978; Sigma-Aldrich). The antibody against β-actin was diluted to 1:10,000 in 5% (w/v) non-fat milk in TBST. None of the agents tested had any effect on β-actin expression, demonstrating its utility as an appropriate loading control. Densitometric analysis was performed using ChemiDoc Image Lab Software (BioRad, Hercules, California). Data were normalized to the corresponding β-actin standards.

2.4. Immunofluorescence and confocal microscopy

The immunofluorescence and confocal microscopy was performed as described previously [15]. Primary antibodies used included those against: NDRG1 (Cat. # 9485, Cell Signaling Technology or Cat. # H00010397-M03, Novus Biologicals, CO), LC3 (Cat# MBPM036; Abacus, Brisbane, Australia) and PSMD9 (Cat. # ab58115; Abcam Inc.). The secondary anti-goat Alexa Fluor® 488 (Cat. # A-11055; Thermo Fisher Scientific) and/or anti-rabbit Alexa Fluor® 594 (Cat. # 8889; Cell Signaling Technology), or anti-mouse Alexa Fluor® 594 (Cat. # A-11058; Thermo Fisher Scientific). Images were taken and processed using a ZEISS LSM 800 Confocal Microscope plus Airyscan (Carl Zeiss Microscopy, Oberkochen, Germany). Fluorescence intensities from immunofluorescence images were quantified using ImageJ software (NIH, Bethesda, MA). In order to quantify co-localization, Pearson's coefficients and the average intensities from co-localized pixels were calculated using ImageJ (NIH).

2.5. Statistics

Experimental data were compared using the Student's paired *t*-test. Results were considered statistically significant when $p < 0.05$. Results are presented as the mean ± standard deviation (S.D.).

3. Results

3.1. Proteasomal and autophagic inhibitors differentially effect the expression of NDRG1 bands

Multiple molecular weight bands for NDRG1 (*via* immunoblot analysis) have been observed in many previous studies, in particular

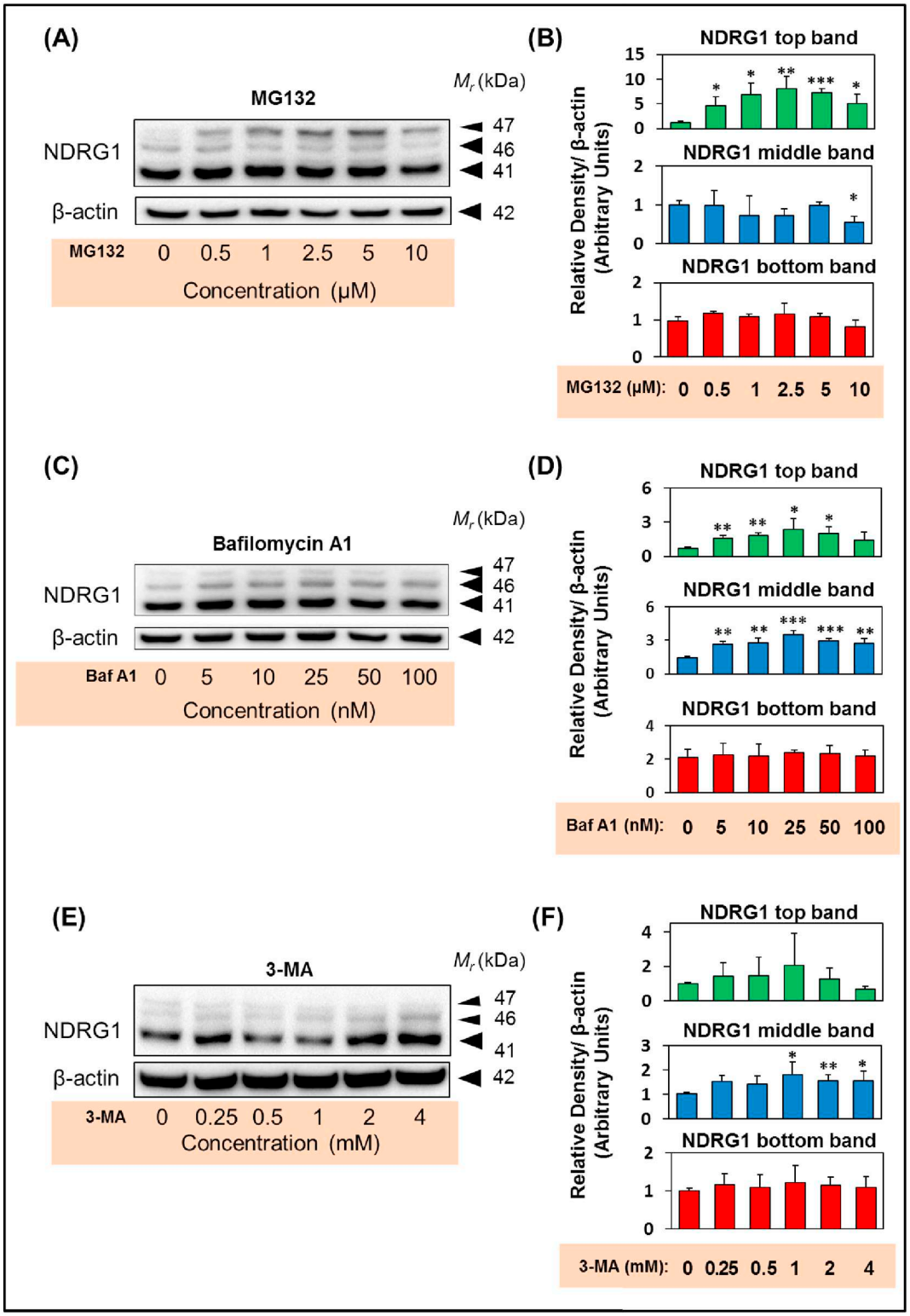

Fig. 1. Proteasomal and autophagy inhibitors increase levels of the top and middle NDRG1 isoforms, respectively. (A, C, E) PANC1 cells were incubated with increasing concentrations of MG132 (0.5–10 μM), Bafilomycin A1 (Baf A1; 5–100 nM), or 3-methyladenine (3-MA; 0.25–4 mM) for 24 h/37 °C. Immunoblotting was then performed to investigate levels of different NDRG1 isoforms. (B, D, F) Densitometric analysis (arbitrary units) of results in (A), (C) or (E), respectively. β-actin was used as a loading control. Results are shown as mean ± S.D. (3 experiments): $^{*}p < 0.05$, $^{**}p < 0.01$; $^{***}p < 0.001$ compared to control cells.

41-, 46- and 47-kDa bands were recently reported after examination of six tumor cell-types [15]. However, the exact nature of these bands and their origin still remain unclear. Therefore, studies were initiated to define the mechanisms of their generation by incubation of PANC1 pancreatic cancer cells with inhibitors of two major protein processing pathways, namely, the proteasomal and autophagic pathways.

The PANC1 cell-type was initially utilized as we have previously observed different NDRG1 isoforms and their response to inducing agents, such as Dp44mT [39,45,46], using these cells. In the first set of studies, PANC1 cells were incubated for 24 h/37 °C in the presence and

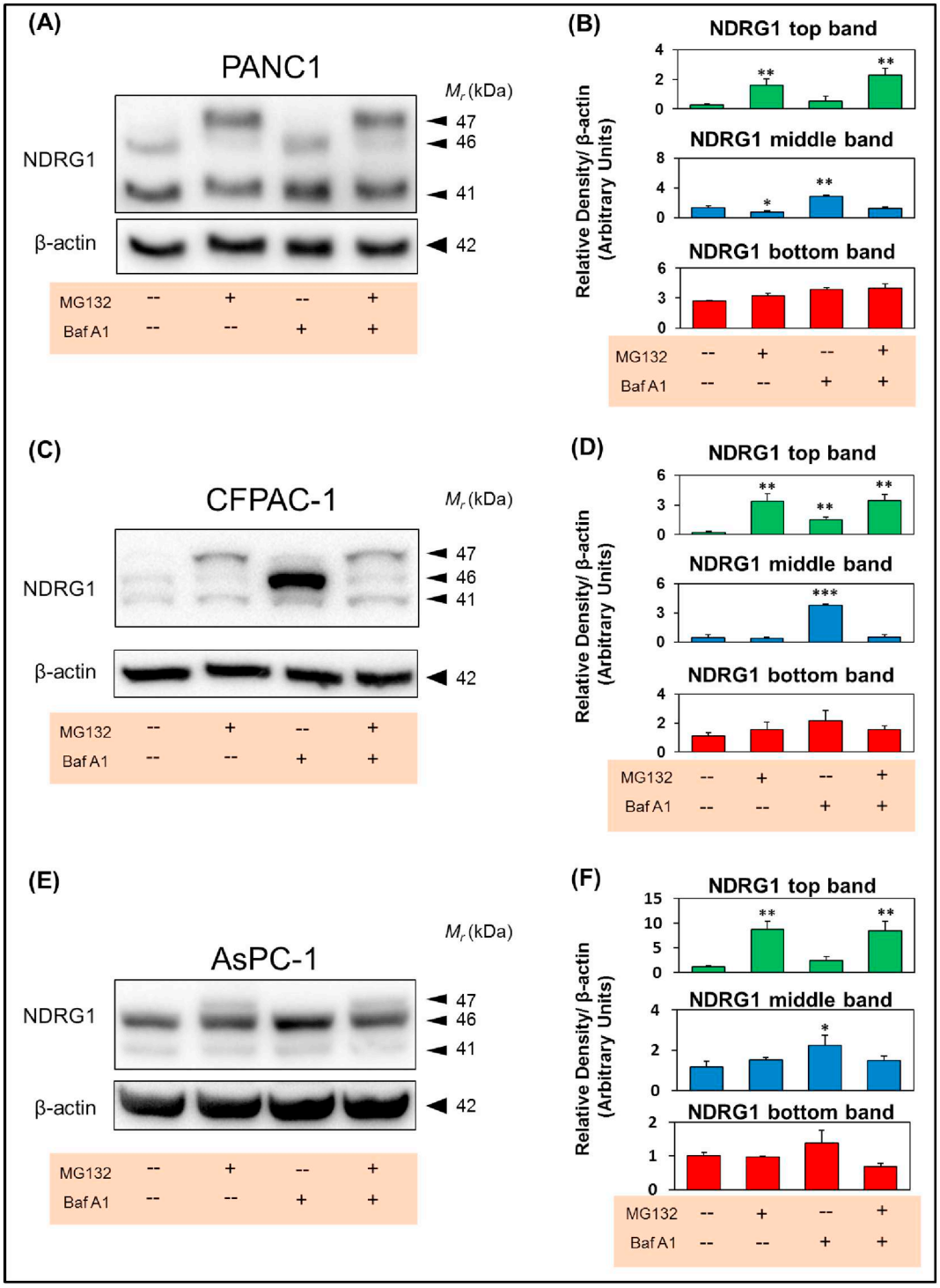

Fig. 2. Proteasomal degradation of the NDRG1 top band is followed by autophagic degradation of the middle NDRG1 band. (A) PANC1, (C) CFPAC-1, or (E) AsPC-1 cells were incubated with either MG132 (10 μM), Baf A1 (100 nM), or both for 24 h/37 °C. (A, C, E) Immunoblotting was then performed to investigate levels of different NDRG1 isoforms. (B, D, F) Densitometric analysis (arbitrary units) of the results in (A), (C) or (E), respectively. β-actin was used as a loading control. Results are shown as mean ± S.D. (3 experiments): *$p < 0.05$; **$p < 0.01$; ***$p < 0.001$ compared to control cells.

absence of the well-established proteasomal inhibitor, MG132 (0.5–10 μM; [47]). Immunoblot analysis revealed three NDRG1 bands under all conditions, defined here as the bottom (~41-kDa), middle (~46-kDa) and top (~47-kDa) NDRG1 bands (Fig. 1A, B). Relative to the control, there was a marked and significant ($p < 0.001$–0.05) increase in the top NDRG1 band at ~47-kDa, with all MG132 concentrations, with a maximum effect occurring at 2.5 μM MG132. At an MG132 concentration of 10 μM, there was a slight, but significant ($p < 0.05$) decrease in the middle NDRG1 band. The levels of the bottom NDRG1 band were not altered by MG132 at all concentrations. Overall, these results in Fig. 1A suggest a role for the proteasome in modulating predominately the top NDRG1 isoform.

Next, PANC1 cells were incubated with the well-established autophagy inhibitors, Bafilomycin A1 (Baf A1; Fig. 1C, D), or 3-methyladenine (3-MA; Fig. 1E, F). Of note, Baf A1 is a late-stage autophagic inhibitor, which inhibits autophagosome-lysosome fusion and also

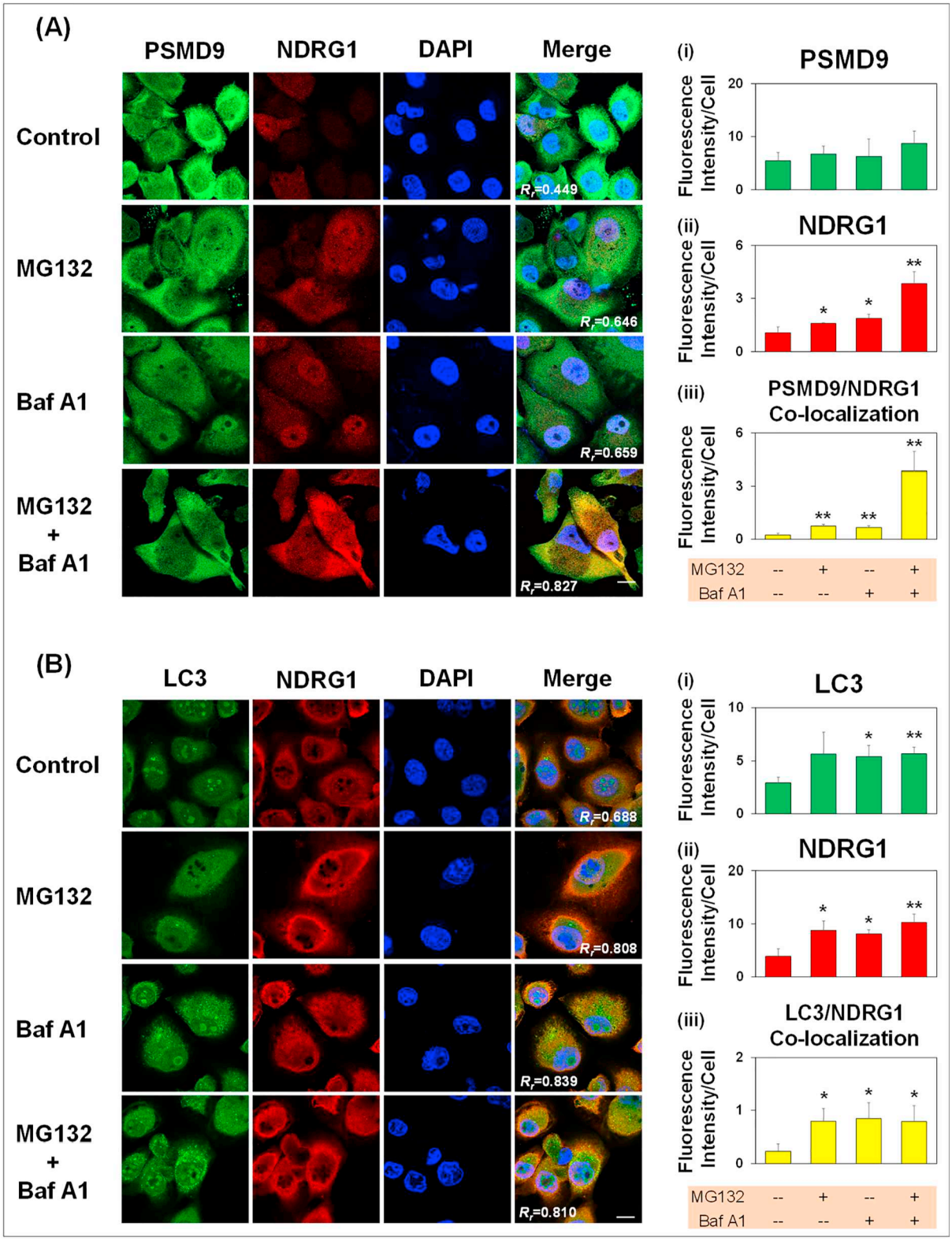

Fig. 3. Simultaneous inhibition of proteasomal and autophagic pathways leads to increased co-localization of NDRG1 with PSMD9 and LC3. (A) PANC1 cells were incubated with either MG132 (10 μM), Baf A1 (100 nM), or both for 24 h/37 °C. Immunofluorescence images show staining for PSMD9 (green), NDRG1 (red) and DAPI for nuclei (blue). Images are representative from 3 experiments performed. Quantification of: (i) pixel intensity of PSMD9; (ii) NDRG1; and (iii) co-localization of PSMD9 and NDRG1 was performed using ImageJ software. (B) PANC1 cells were incubated with either MG132 (10 μM), Baf A1 (100 nM), or both for 24 h/37 °C. Immunofluorescence images demonstrate staining for LC3 (green), NDRG1 (red) and DAPI for nuclei (blue). Images are representative from 3 experiments performed. Quantification of: (i) pixel intensity of LC3; (ii) NDRG1; and (iii) co-localization of LC3 and NDRG1 was performed using ImageJ software. Quantification of the results are shown as mean ± standard deviation (3 experiments): $*p < 0.05$, $**p < 0.01$, relative to the respective control. The scale bar in the bottom right hand corner of the first image in (A) and (B) represents 10 μm and is the same across all images. Pixel intensity and co-localization analysis utilized a total of 11–28 cells over 3 experiments. Co-localization was measured by Pearson's correlation coefficient (R_r).

neutralizes the acidic pH of lysosomes [38,48]. Hence, it can inhibit both macroautophagy as well as chaperone-mediated autophagy [48]. In contrast, 3-MA inhibits phagophore formation, and thus, only inhibits macroautophagy [46]. Incubation of cells with increasing concentrations of Baf A1 led to a slight, but significant ($p < 0.01$–0.05), increase in levels of the top NDRG1 band up to 50 nM, with no significant ($p > 0.05$) change observed at 100 nM Baf A1 (Fig. 1C, D). Incubation of cells with Baf A1 also markedly and significantly ($p < 0.001$–0.01) increased the middle NDRG1 band at ~46-kDa, relative to the control, with a maximum effect being observed at 25 nM (Fig. 1C, D). There was no alteration of the bottom NDRG1 band at any Baf A1 concentration.

Incubation of cells with 3-MA (0.25–4.0 mM) significantly ($p < 0.01$–0.05) increased the middle NDRG1 band, but only between 1 and 4 mM (Fig. 1E, F). On the other hand, there was no significant change in the top or bottom NDRG1 bands after incubation with 3-MA (Fig. 1E, F). Collectively, these results suggest that proteasomal and autophagic processing leads to the regulation of top and middle NDRG1 isoforms, respectively, with no marked effect on the bottom band. Based on these studies, all future experiments were performed using 10 μM MG132, 100 nM Baf A1, or 2 mM 3-MA, as these concentrations were optimal in differentially detecting alterations in the top (MG132) or middle (Baf A1 and 3-MA) NDRG1 bands.

3.2. The proteasomal inhibitor, Epoxomycin, has a similar effect to MG132 and increases the top NDRG1 band

The effect of MG132 on NDRG1 isoform expression in PANC1 cells was also compared to another well-established and most selective proteasomal inhibitor commercially available, namely Epoxomycin [47]. Similarly to MG132, incubation with Epoxomycin (5 μM) led to a marked and significant ($p < 0.001$) increase in the top NDRG1 band *versus* the control (Supplemental Fig. 1). As MG132 has also been reported to inhibit calpain and cathepsin activity, in addition to the proteasome [47,49], the effect of the calpain and cathepsin inhibitor, E64D (25 μg/mL) [47], was also examined as a relative control. Unlike MG132, after incubation of PANC1 cells with E64D, there was no significant ($p > 0.05$) increase in the top NDRG1 band relative to the control (Supplemental Fig. 1). However, there was a significant ($p < 0.05$) increase in the middle NDRG1 band after incubation with E64D compared to the control. This latter increase could be due to the known inhibition of lysosomal cathepsins by E64D [50], resulting in similar effects to the autophagic inhibitor, Baf A1 (Fig. 1C, D). Again, there was no consistent change observed in the bottom NDRG1 band after incubation with any of the inhibitors. Taken together, these results suggest that proteasomes and autophagy are involved in the processing of the top and middle NDRG1 bands, respectively.

3.3. Proteasomal processing precedes autophagic metabolism of NDRG1

Next, the effect of combining the proteasomal inhibitor and autophagic inhibitor on NDRG1 isoform expression was examined (Fig. 2). PANC1 cells were incubated with either MG132 (10 μM) or Baf A1 (100 nM) alone, or in combination, for 24 h/37 °C. As shown above (Fig. 1A–D), MG132 or Baf A1 had the same effects on the top and middle NDRG1 bands (Fig. 2A). However, when cells were co-incubated with MG132 and Baf A1, only the top NDRG1 band was significantly ($p < 0.01$) increased. This observation suggests that proteasomal activity was required to generate the middle NDRG1 band, which may then be processed by autophagy. There was no significant change in the levels of the bottom NDRG1 band, under all incubation conditions.

As pancreatic cancer is a highly heterogeneous disease, the effects of the proteasomal and autophagic inhibitors on NDRG1 isoforms in several different pancreatic cancer cell-types, namely CFPAC-1 (Fig. 2C, D) and AsPC-1 cells (Fig. 2E, F), were also investigated. Similar to PANC1 cells, incubation of CFPAC-1 or AsPC-1 cells with MG132 or Baf A1 resulted in a significant ($p < 0.001$–0.05) increase in the top and middle NDRG1 bands, respectively, relative to the control. Again, co-incubation with the combination of MG132 and Baf A1 led only to a significant ($p < 0.01$) increase in the top NDRG1 band, relative to the control, in both cell-types examined (Fig. 2C–F). These results suggest similar mechanisms of NDRG1 processing in all pancreatic cancer cell-types examined. As NDRG1 function has been thoroughly examined in PANC1 cells [4,39,45,51], further studies were performed using this cell-type.

3.4. Concurrent inhibition of proteasomal and autophagic pathways leads to increased co-localization of NDRG1 with the proteasomal marker, PSMD9, and autophagic marker, LC3

As the studies in Figs. 1 and 2 demonstrated an important role of both proteasomal and autophagic pathways in NDRG1 processing, further studies were initiated to examine the effects of proteasomal and autophagic inhibition on the intracellular localization of NDRG1. PANC1 cells were incubated with either MG132 (10 μM), Baf A1 (100 nM), or both for 24 h/37 °C. Cells were then assessed by immunofluorescence using confocal microscopy (Fig. 3).

In the first set of studies (Fig. 3A), PANC1 cells were probed for the known proteasomal marker, PSMD9 (green) [52,53], NDRG1 (red) and DAPI (blue). The NDRG1 antibody utilized in confocal microscopy detects the total form of the protein and does not discriminate between top, middle and bottom isoforms detected in immunoblot analysis [15]. Levels of PSMD9 (green intensity) were not significantly ($p > 0.05$) affected under all incubation conditions compared to control cells (Fig. 3A). Assessing NDRG1 levels, both nuclear and cytoplasmic staining was observed under all incubation conditions, which is consistent with previous observations with this protein [15,54]. There was a significant ($p < 0.05$) increase in NDRG1 levels after incubation with either MG132 or Baf A1 compared to control cells. There was a marked and significant ($p < 0.01$) increase in NDRG1 levels after incubation with combination of MG132 and Baf A1 (Fig. 3A). The co-localization of PSMD9 (green) and NDRG1 (red) was visualized as yellow fluorescence in the merged images. Notably, quantification of co-localization demonstrated a significant ($p < 0.01$) increase in co-localization of PSMD9 and NDRG1 under all treatment conditions relative to the control (Fig. 3A). This co-localization was also evident by measurement of the Pearson's correlation coefficient (R_r), that demonstrated higher co-localization after incubation of cells with MG132 (R_r: 0.646) or Baf A1 (R_r: 0.659) *versus* the control (R_r: 0.449). More prominent co-localization was observed after incubation with both MG132 and Baf A1 (R_r: 0.827) compared to control cells (R_r: 0.449).

Next, PANC1 cells were probed for the autophagic marker, LC3 (green) [38], NDRG1 (red) and DAPI (blue; Fig. 3B). Examining LC3 levels, there was a significant ($p < 0.01$–0.05) increase in the intensity of LC3 after incubation of cells with Baf A1, or MG132 and Baf A1 (Fig. 3B). Notably, there was a marked increase in punctuate cytoplasmic staining under these incubation conditions, which is probably due to increased autophagosomes accumulation due to late-stage (*i.e.*, lysosome-mediated degradation of autophagosomes) inhibition of autophagy by Baf A1 [38,39]. As observed above (Fig. 3A), NDRG1 levels were significantly ($p < 0.01$–0.05) increased after incubation of cells under all treatment conditions (Fig. 3B). Quantification of co-localization demonstrated a significant ($p < 0.05$) increase in co-localization of LC3 and NDRG1 in cells incubated with Baf A1 or MG132 alone or MG132 and Baf A1 (Fig. 3B). This co-localization was also evident by measurement of the Pearson's correlation coefficient (R_r), that was higher in cells incubated with MG132 (R_r: 0.808), Baf A1 (R_r: 0.839), or the combination of MG132 and Baf A1 (R_r: 0.810) compared to the control cells (R_r: 0.688).

Overall, simultaneous inhibition of proteasomal and autophagic

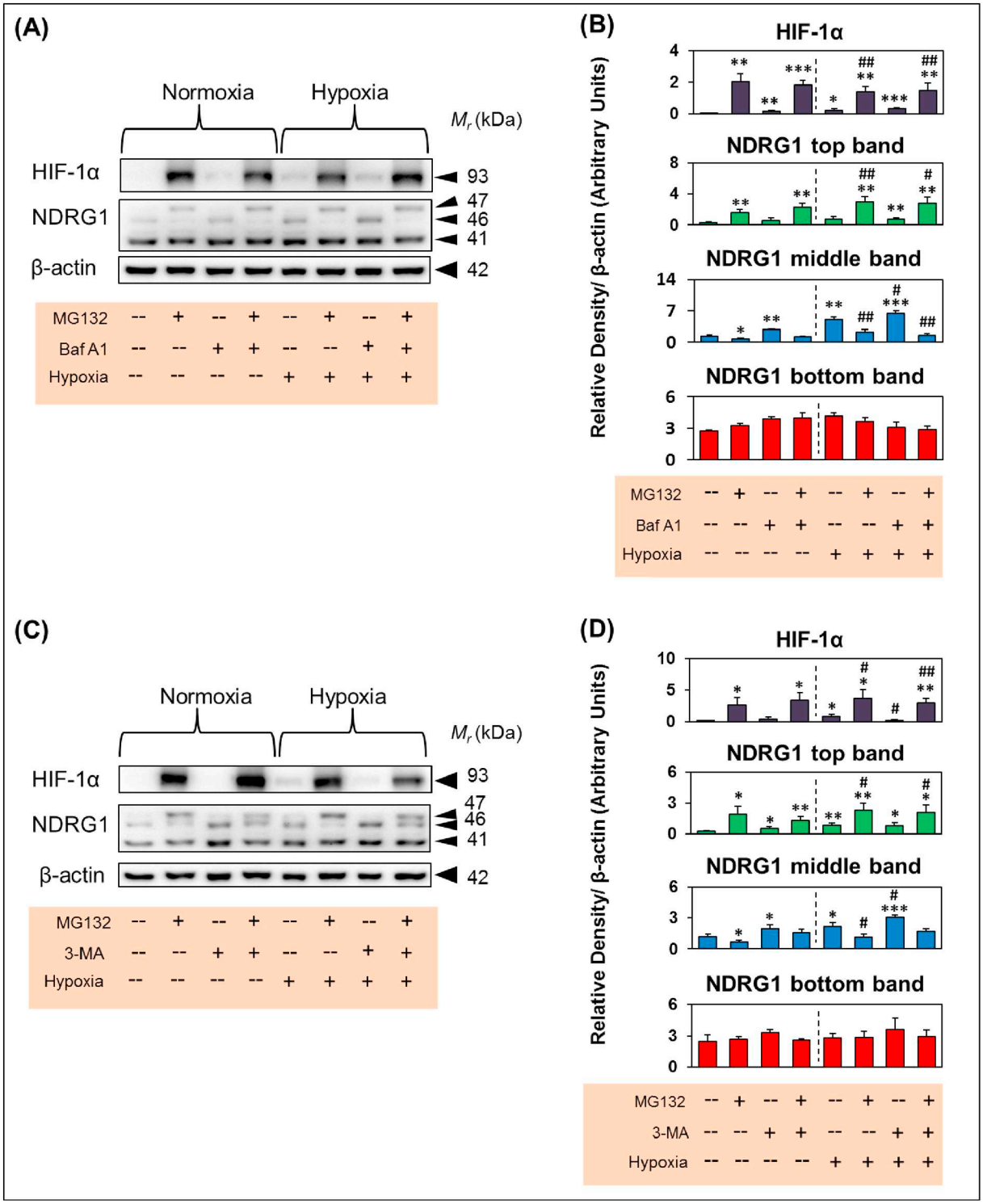

Fig. 4. Proteasomal activity is required for induction of the NDRG1 middle band by the well-characterized physiological inducer, hypoxia. (A) PANC1 cells were incubated with either MG132 (10 μM), Baf A1 (100 nM), or both in the absence or presence of hypoxia (1% O_2) for 24 h/37 °C. Immunoblotting was then performed to investigate levels of hypoxia-inducible factor-1α (HIF-1α) and the different NDRG1 isoforms. (B) Densitometric analysis (arbitrary units) of the results in (A). β-actin was used as a loading control. (C) PANC1 cells were incubated with either MG132 (10 μM), 3-MA (2 mM), or both in the absence or presence of hypoxia (1% O_2) for 24 h/37 °C. Immunoblotting was then performed to investigate levels of hypoxia-inducible factor-1α (HIF-1α) and the different NDRG1 isoforms. (D) Densitometric analysis (arbitrary units) of the results in (C). β-actin was used as a loading control. Results are shown as mean ± S.D. (3 experiments). $^{*}p < 0.05$; $^{**}p < 0.01$; $^{***}p < 0.001$ compared to control cells. $\#p < 0.05$; $\#\#p < 0.01$; compared to hypoxia alone.

pathways results in significant increase in the intensity of NDRG1 and its co-localization with both proteasomes and autophagosomes. These results again underline the important role of both these pathways in NDRG1 processing.

3.5. Proteasomal activity is required for NDRG1 induction by its well-characterized inducer, hypoxia

The effect of MG132 and Baf A1 was further assessed in PANC1 cells

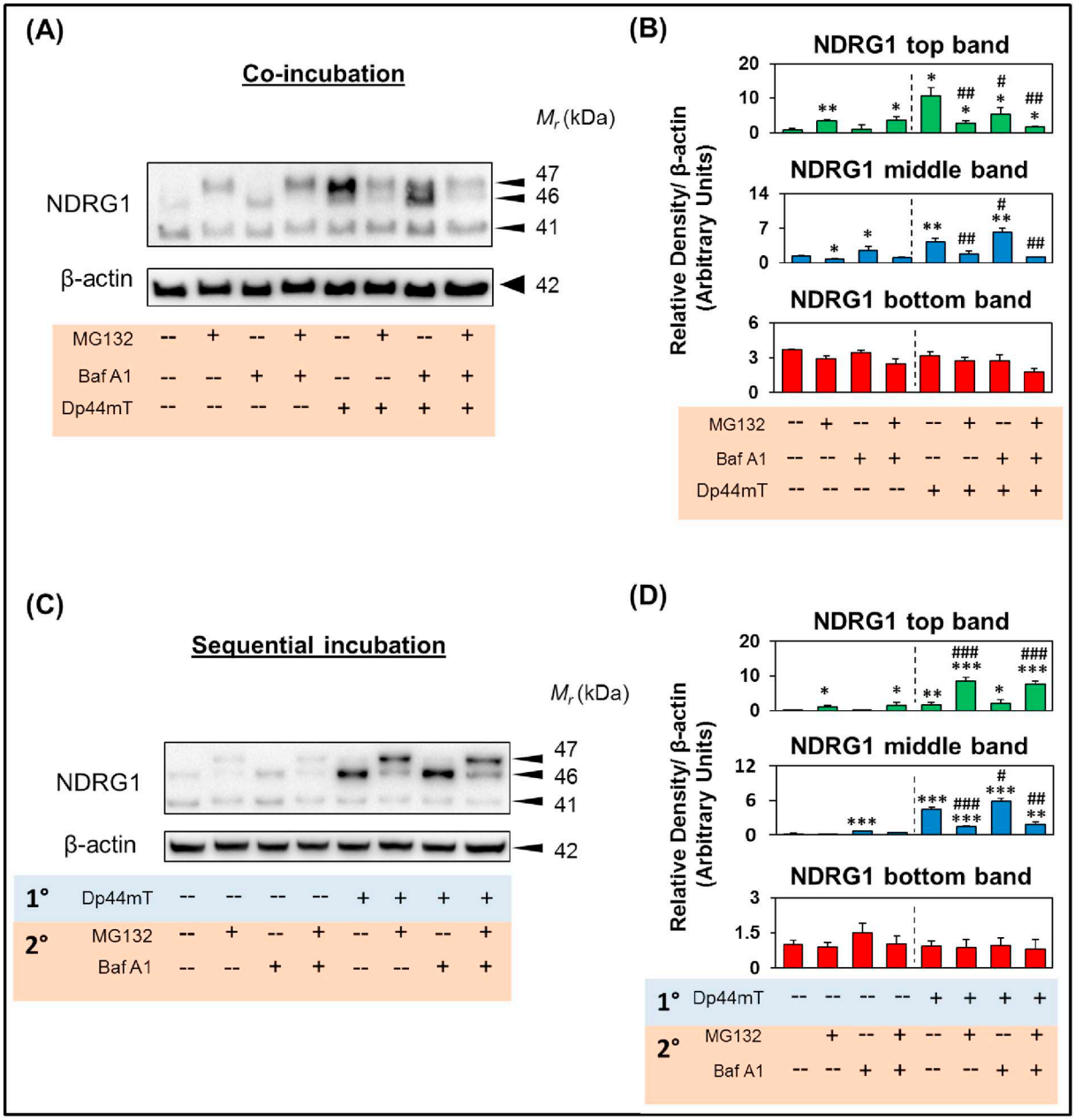

Fig. 5. Proteasomal activity is required for the induction of the top and middle NDRG1 bands by its well-characterized pharmacological inducer, Dp44mT. (A) Co-Incubation Study: PANC1 cells were incubated for 24 h/37 °C with or without Dp44mT (10 μM) in combination with MG132 (10 μM), Baf A1 (100 nM), or both. Immunoblotting was then performed to investigate levels of the different NDRG1 isoforms. (B) Densitometric analysis (arbitrary units) of results in (A). β-actin was used as a loading control. (C) Sequential Incubation Study: First, PANC1 cells were incubated for 24 h/37 °C with or without Dp44mT (10 μM). Second, cells were washed and supplemented with either control medium or medium containing either MG132 (10 μM), Baf A1 (100 nM), or both. Immunoblotting was then performed to investigate levels of the different NDRG1 isoforms. (D) Densitometric analysis (arbitrary units) of the results in (C). β-actin was used as a loading control. Results are shown as mean ± S.D. (3 experiments). *$p < 0.05$; **$p < 0.01$; ***$p < 0.001$ compared to control cells. #$p < 0.05$; ##$p < 0.01$; ###$p < 0.001$ compared to Dp44mT alone.

incubated for 24 h/37 °C under normoxia (21% O_2/5% CO_2), or with the well-established NDRG1-inducer, hypoxia (1% O_2/5% CO_2) [24], that up-regulates NDRG1 through HIF-1α-dependent and -independent mechanisms [22]. Under hypoxic conditions, HIF-1α levels are known to be regulated at the post-translational level *via* the proteasomal degradation pathway [55]. As a positive control for inhibition of proteasomal degradation, studies first assessed HIF-1α expression in the presence of MG132 (10 μM), which significantly ($p < 0.01$) up-regulated HIF1α levels relative to the corresponding normoxic or hypoxic controls (Fig. 4A, B), as demonstrated previously [55]. Further, Baf A1(100 nM) alone in the absence or presence of hypoxia slightly, but significantly ($p < 0.001$–0.01) increased HIF-1α levels relative to the normoxic control (Fig. 4A, B). Combination of Baf A1 (100 nM) and MG132 (10 μM) under normoxia or hypoxia also markedly and significantly ($p < 0.001$–0.01) increased HIF-1α expression. Collectively, these results suggest that inhibition of the proteasome, and to a much lesser extent the lysosome, led to increased HIF-1α expression.

Examining NDRG1 expression in PANC1 cells under hypoxia relative to the corresponding normoxic control, led to a significant ($p < 0.01$) increase in the NDRG1 middle band, but not the top or bottom bands (Fig. 4A, B). Interestingly, the ability of hypoxia to induce expression of the NDRG1 middle band was ablated in the presence of

MG132. However, cells incubated with MG132 under hypoxic conditions were still able to significantly ($p < 0.01$) increase the top NDRG1 band relative to the normoxic and hypoxic controls (Fig. 4A, B).

Incubation of cells with hypoxia and Baf A1 resulted in a significant ($p < 0.001$–0.05) increase in the middle NDRG1 band compared to control cells incubated under normoxia or hypoxia (Fig. 4A, B). Notably, co-incubation of cells with MG132 and Baf A1 under hypoxia, resulted in significantly ($p < 0.05$) increased levels of the top NDRG1 band compared to hypoxia alone. Moreover, co-incubation with these latter agents led to a marked and significant ($p < 0.01$) suppression in the levels of the middle NDRG1 band under these conditions compared to hypoxia alone. There was no significant ($p > 0.05$) change in the bottom NDRG1 band under all incubation conditions. Taken together, these results indicate that proteasome activity (*i.e.*, cells incubated without MG132) is required to convert the top NDRG1 band to the middle isoform, which can be subsequently degraded by autophagy.

Studies in the presence of hypoxia or normoxia then examined the effect of MG132 (10 μM) and another well-characterized autophagic inhibitor, 3-MA (2 mM), that only inhibits macroautophagy and unlike Baf A1 does not inhibit chaperone-mediated autophagy [56] (Fig. 4C, D). In contrast to Baf A1 (Fig. 4A, B), 3-MA was unable to increase HIF-1α levels under normoxia or hypoxia, which is consistent with the fact that HIF-1α is degraded by chaperone-mediated autophagic degradation, but not macroautophagy [57].

Considering NDRG1 expression, 3-MA significantly ($p < 0.05$) increased the middle band relative to the normoxic control (Fig. 4C, D). However, co-incubation with MG132 and 3-MA under normoxia resulted in a significant ($p < 0.01$) increase in the top NDRG1 band relative to the normoxic control, while there was a slight, but not significant increase in the middle NDRG1 band (Fig. 4C, D). Under hypoxic conditions, co-incubation with MG132 and 3-MA, resulted in similar effects to those observed under normoxia, with both the top and middle NDRG1 bands becoming apparent.

Collectively, in the presence and absence of the NDRG1-inducer, hypoxia, these results above suggest the top NDRG1 band is processed to the middle band by the proteasome, which was further degraded by macroautophagy. Interestingly, combination of MG132 and 3-MA results in accumulation of the top NDRG1 band and a slight increase in the middle band. This observation suggests that while 3-MA inhibits macroautophagy, its inability to block chaperone-mediated autophagy may result in some conversion of the top band into the middle band by this process. The decrease in the intensity of the top band in the presence of 3-MA and MG132, relative to that observed with MG132 alone (Fig. 4C, D), supports this hypothesis.

3.6. Active proteasomal activity is also required to induce NDRG1 by its potent inducer, Dp44mT

Next, we also examined the effect of another potent NDRG1-inducer, Dp44mT, on NDRG1 isoforms [22,27,28,58]. PANC1 cells were incubated for 24 h/37 °C with Dp44mT (10 μM) in the absence or presence of MG132 (10 μM), Baf A1 (100 nM), or both (Fig. 5A). Incubation with Dp44mT alone led to a marked and significant ($p < 0.01$–0.05) increase in the levels of both the top and middle NDRG1 bands compared to control cells (Fig. 5A, B).

Co-incubation of cells with MG132 and Dp44mT significantly ($p < 0.01$) reduced the ability of Dp44mT to induce the middle and top NDRG1 bands compared to Dp44mT alone (Fig. 5A, B). On the other hand, co-incubation of cells with Baf A1 and Dp44mT, significantly ($p < 0.05$) reduced the levels of the top NDRG1 band, but significantly ($p < 0.05$) increased the levels of middle NDRG1 band compared to Dp44mT alone. Finally, co-incubation of cells with MG132, Baf A1 and Dp44mT significantly ($p < 0.01$) abrogated the ability of Dp44mT to induce the middle and top NDRG1 bands (Fig. 5A, B). Again, there was no significant change observed in the bottom NDRG1 band under all incubation conditions. These results demonstrate the importance of proteasome activity for induction of NDRG1 bands in PANC1 cells.

To further ascertain the role of proteasomal activity in Dp44mT-mediated up-regulation of the middle and top NDRG1 bands, studies were initiated where PANC1 cells were first incubated for 24 h/37 °C with Dp44mT to induce NDRG1. These cells were then washed and sequentially incubated for 24 h/37 °C with control medium alone, MG132, Baf A1, or both (Fig. 5C, D). Incubation of cells with Dp44mT (24 h) followed by control medium (24 h) led to a significant ($p < 0.001$) increase in the middle NDRG1 band compared to control cells (Fig. 5C, D). This is consistent with the hypothesis that the NDRG1 top band is converted to the middle band, potentially by a proteasome-dependent mechanism.

Sequentially incubating Dp44mT followed by MG132 led to a marked and significant ($p < 0.001$) increase in the top NDRG1 band relative to the control (Fig. 5C, D). Moreover, sequential incubation of Dp44mT followed by Baf A1 resulted in a slight, but significant ($p < 0.05$) increase in the middle NDRG1 band compared to cells incubated with Dp44mT alone (Fig. 5C, D). Incubation with Dp44mT followed by co-incubation with MG132 and Baf A1 resulted in a marked and significant ($p < 0.001$) increase in the top NDRG1 band and a significant ($p < 0.01$) decrease in the middle NDRG1 band relative to Dp44mT alone (Fig. 5C, D). Again, these various incubation conditions led to no significant effect on the bottom NDRG1 band.

Collectively, these studies indicate that proteasomal activity is required for Dp44mT to increase the levels of the top and middle NDRG1 bands. Once induced, NDRG1 bands are processed and degraded by proteasomal and then autophagic pathways.

3.7. Middle and top NDRG1 bands correlate with phosphorylated NDRG1 protein forms

A previous report suggested that NDRG1 phosphorylation is involved in its proteasomal degradation [20]. As we observed an increase in the top or middle NDRG1 band upon incubation with proteasomal or autophagic inhibitors respectively, the effect of both proteasomal and autophagy inhibitors were then examined on the levels of two well-established phosphorylated forms of NDRG1, *i.e.*, p-NDRG1 (Ser330) and p-NDRG1 (Thr346) [16].

Initially, PANC1 cells were either incubated with MG132 (10 μM), Baf A1 (100 nM), or both in the presence or absence of Dp44mT (10 μM) for 24 h/37 °C. In total, three bands (41-, 46- and 47-kDa) of p-NDRG1 (Ser330) were observed, with the bottom band only being observed after incubation with Dp44mT (Fig. 6A). Under all incubation conditions, the levels of the top and middle p-NDRG1 (Ser330) bands (Fig. 6A, B) generally corresponded with top and middle bands of total NDRG1 (Fig. 5A, B).

In terms of p-NDRG1 (Thr346), only two major bands were observed at 41- and 47-kDa (Fig. 6A, C). The relative levels of the top band of p-NDRG1 (Thr 346) (Fig. 6A, C) corresponded with the top band of total NDRG1 under these same incubation conditions (Fig. 5A, B). In contrast, the bottom p-NDRG1 band (Thr346) was observed only after incubation with Dp44mT (Fig. 6A, C), relative to the bottom band of total NDRG1 that was observed under all conditions (Fig. 5A, B).

Next, experiments were also performed with sequential incubation of PANC1 cells in the presence and absence of Dp44mT (10 μM) for 24 h/37 °C, followed by washing, and then incubation with MG132 (10 μM), Baf A1 (100 nM), or both for 24 h/37 °C. The levels of the top and middle bands of p-NDRG1 (Ser330) (Fig. 6D, E) correlated with levels of the corresponding total NDRG1 bands (Fig. 5C, D). In contrast, the levels of the bottom p-NDRG1 (Ser330) band (Fig. 6D, E) was different compared to the bottom band of total NDRG1 observed under similar incubation conditions (Fig. 5C, D).

The levels of the top band of p-NDRG1 (Thr346) (Fig. 6D, F) correlated with the levels of the top total NDRG1 band (Fig. 5C, D). Again, the levels of the bottom p-NDRG1 (Thr346) band (Fig. 6D, F) were different compared to the bottom band of total NDRG1 observed under

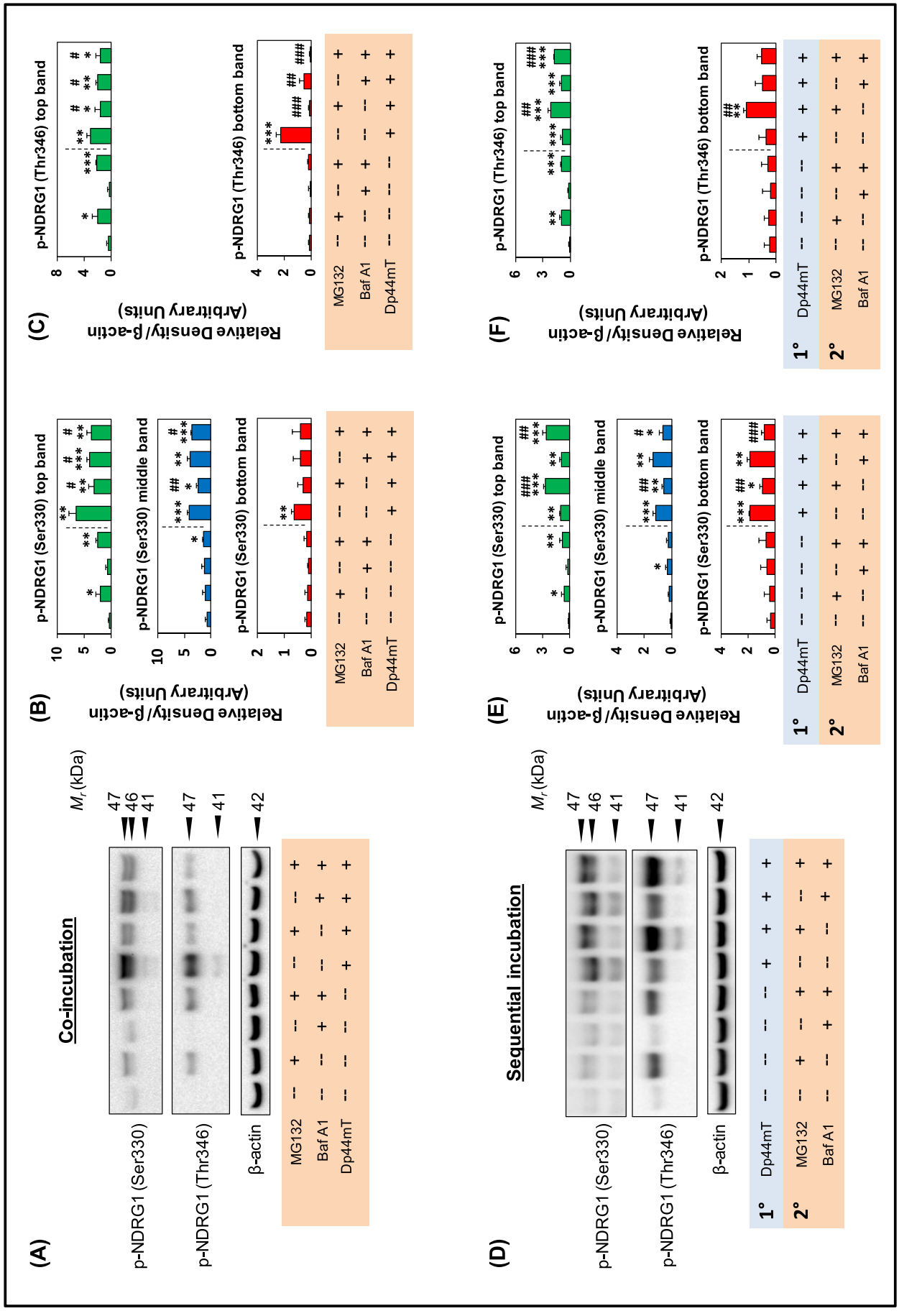

Fig. 6. Levels of the middle and top total NDRG1 bands correlate with levels of the phosphorylated NDRG1 protein isoforms. (A) Co-Incubation Study: PANC1 cells were incubated for 24 h/37 °C with or without Dp44mT (10 μM) in combination with MG132 (10 μM), Baf A1 (100 nM), or both. Immunoblotting was then performed to investigate levels of the different isoforms of p-NDRG1 (Ser330) and p-NDRG1 (Thr346). (B, C) Densitometric analysis (arbitrary units) of results in (A). β-actin was used as a loading control. (D) Sequential Incubation: First, PANC1 cells were incubated for 24 h/37 °C with or without Dp44mT (10 μM). Second, cells were washed and supplemented with either control medium or medium containing with MG132 (10 μM), Baf A1 (100 nM), or both. Immunoblotting was then performed to investigate levels of the different isoforms of p-NDRG1 (Ser330) and p-NDRG1 (Thr346). (E, F) Densitometric analysis (arbitrary units) of the results in (D). β-actin was used as a loading control. Results are shown as mean ± S.D. (3 experiments). $^{*}p < 0.05$; $^{**}p < 0.01$; $^{***}p < 0.001$ compared to control cells. $\#p < 0.05$; $\#\#p < 0.01$; $\#\#\#p < 0.001$ compared to Dp44mT alone.

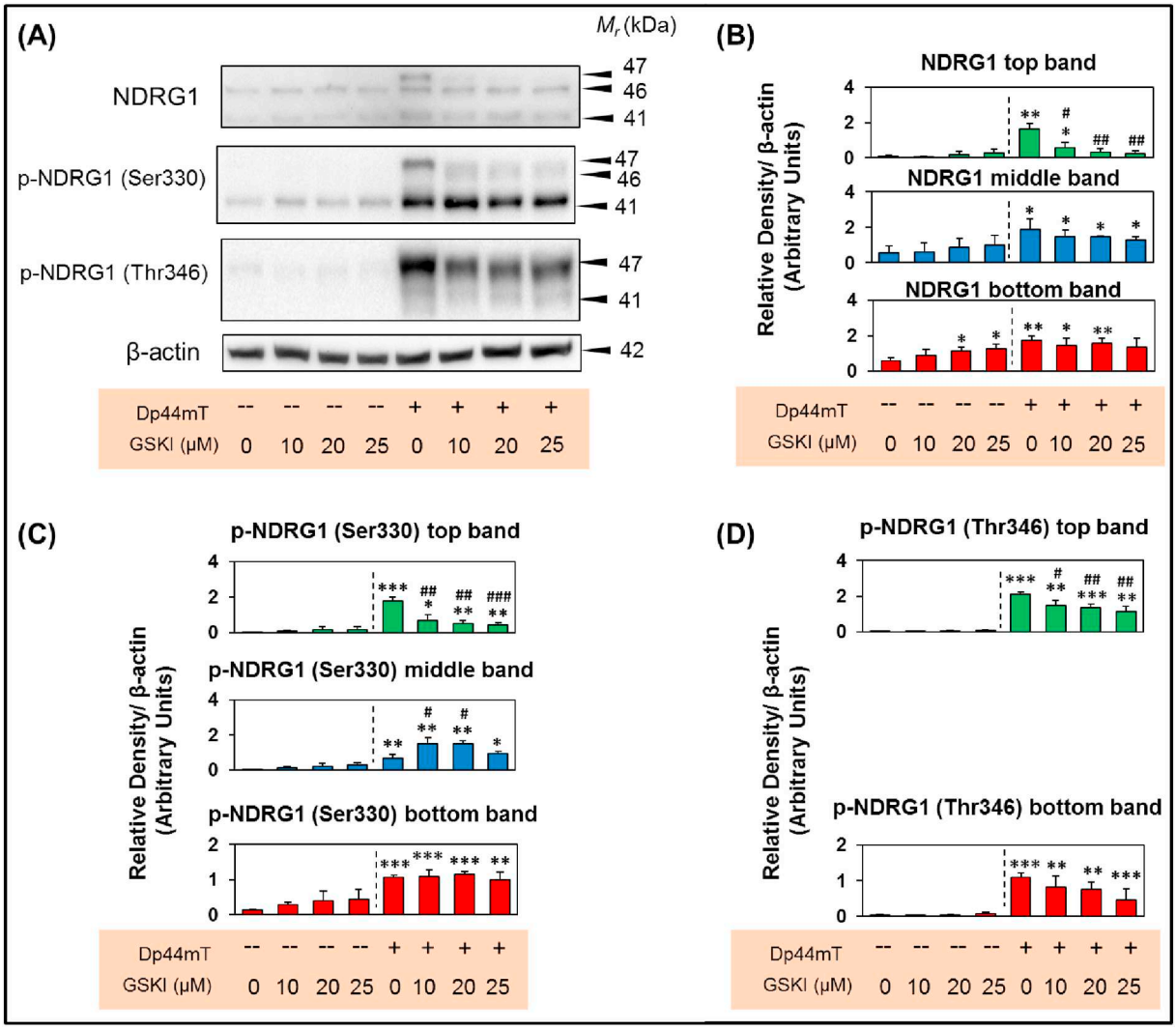

Fig. 7. Inhibition of the upstream kinase, GSK3β, by the inhibitor SB216763, leads to reduction in the Dp44mT-induced top NDRG1 band. (A) PANC1 cells were incubated for 24 h/37 °C with or without Dp44mT (10 μM) in combination with the GSK3β inhibitor (SB216763; GSKI; 10–25 μM). Immunoblotting was then performed to investigate levels of the different isoforms of NDRG1, p-NDRG1 (Ser330) and p-NDRG1 (Thr346). (B-D) Densitometric analysis (arbitrary units) of the results in (A). β-actin was used as a loading control. Results are shown as mean ± S.D. (3 experiments). *$p < 0.05$; **$p < 0.01$; ***$p < 0.001$ compared to control cells. #$p < 0.05$; ##$p < 0.01$; ###$p < 0.001$ compared to Dp44mT alone.

similar incubation conditions (Fig. 5C, D). Taken together, the top and middle NDRG1 bands potentially represent NDRG1 isoforms phosphorylated at Ser330 or Thr346, which are differentially processed.

3.8. Inhibition of upstream kinases, SGK1 and GSK3β, leads to reduction in Dp44mT-induced top NDRG1 band

As our results above indicate that all NDRG1 bands are, at least in part, phosphorylated forms of NDRG1 (Figs. 5 and 6), studies were initiated to examine the effect of the two well-known upstream kinases of NDRG1, *i.e.*, SGK1 and GSK3β [16], on the different NDRG1 bands. The NDRG1-inducer Dp44mT (10 μM) was used to induce NDRG1 expression in PANC1 cells. The cells were incubated in the absence and presence of Dp44mT (10 μM) with increasing concentrations of either the GSK3β-inhibitor (*i.e.*, SB216763; GSKI; 10–25 μM; Fig. 7A–D; [59]) or SGK1-inhibitor (*i.e.*, GSK650394; SGKI; 10–25 μM; Fig. 8A–D; [60]).

In cells incubated without Dp44mT, there was no significant effect of GSKI alone (10–25 μM; Fig. 7A, B) or SGKI alone (10–25 μM; Fig. 8A, B) on any NDRG1 bands. As shown previously, Dp44mT alone was able to significantly ($p < 0.001$–0.05) increase the levels of top and middle total NDRG1 bands relative to the untreated control (Figs. 7A, B; 8A, B). There was significant ($p < 0.001$–0.05) dose-dependent suppression in Dp44mT-induced levels of the top NDRG1 band after co-incubation with increasing concentrations of either GSKI (Fig. 7A, B) or SGKI (Fig. 8A, B). There was no significant ($p > 0.05$) effect of either GSKI (Fig. 7A, B) or SGKI (Fig. 8A, B) on the Dp44mT-induced levels of middle or bottom NDRG1 band.

Examining the phosphorylated NDRG1 bands in the absence of Dp44mT, neither GSKI or SGKI had any significant effect on all p-NDRG1 (Ser330) and p-NDRG1 (Thr346) bands (Figs. 7A, C, D; 8A, C, D). The NDRG1-inducer, Dp44mT, was able to significantly ($p < 0.001$–0.01) increase the levels of all bands detected for both p-NDRG1 (Ser330) and p-NDRG1 (Thr346) (Figs. 7A, C, D; 8A, C, D). Co-incubation of Dp44mT-treated cells with either GSKI (Fig. 7A, C, D) or SGKI (Fig. 8A, C, D) was able to significantly ($p < 0.001$–0.05) suppress the levels of the Dp44mT-induced top p-NDRG1 (Ser330) and p-NDRG1 (Thr346) bands in a dose-dependent manner. In contrast to total NDRG1 levels (Figs. 7A, B; 8A, B), at lower concentrations (10–20 μM), GSKI and SGKI led to a slight, but significant ($p < 0.05$) increase in the Dp44mT-induced middle band of p-NDRG1 (Ser330), while there was no significant ($p > 0.05$) effect observed at a higher inhibitor concentration of 25 μM (Figs. 7A, C; 8A, C). However, both

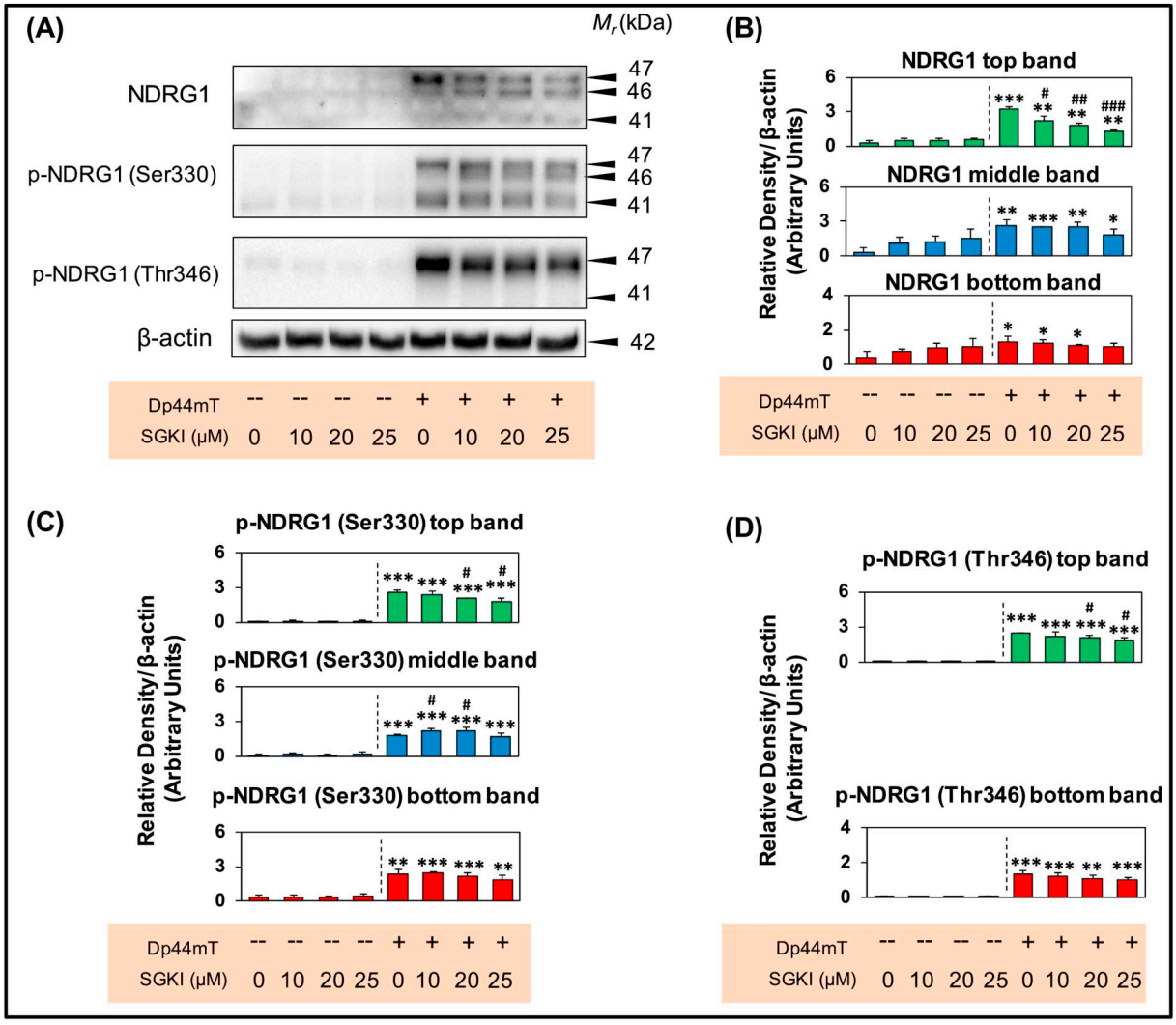

Fig. 8. Inhibition of the upstream kinase, SGK1, by the inhibitor GSK650394, also suppresses the Dp44mT-induced top NDRG1 band. (A) PANC1 cells were incubated for 24 h/37 °C with or without Dp44mT (10 μM) in combination with the SGK1 inhibitor (GSK650394; SGKI; 10–25 μM). Immunoblotting was then performed to investigate levels of the different isoforms of NDRG1, p-NDRG1 (Ser330) and p-NDRG1 (Thr346). (B–D) Densitometric analysis (arbitrary units) of the results in (A). β-actin was used as a loading control. Results are shown as mean ± S.D. (3 experiments). *$p < 0.05$; **$p < 0.01$; ***$p < 0.001$ compared to control cells. #$p < 0.05$; ##$p < 0.01$; ###$p < 0.001$ compared to Dp44mT alone.

GSKI and SGKI did not have any significant effect on the Dp44mT-induced bottom bands of p-NDRG1 (Ser330) and p-NDRG1 (Thr346) (Figs. 7A, C, D; 8A, C, D).

Collectively, the major finding from these studies in Figs. 7 and 8 is that both GSKI and SGKI are involved in inhibiting phosphorylation of the top band, or alternatively, increasing degradation/processing of the Dp44mT-induced top NDRG1 band.

3.9. Inhibition of GSK3β results in the proteasome-independent degradation of top NDRG1 band

As both GSKI and SGKI decreased levels of the Dp44mT-induced top NDRG1 band (Figs. 7, 8), further studies were initiated to examine the mechanism of this effect (Figs. 9, 10). As previous results indicated that NDRG1 is processed/degraded *via* both the proteasome and lysosomal pathways (Figs. 1, 2A), studies were initiated to determine the effect of proteasomal or lysosomal inhibition after suppression of the top NDRG1 band by the GSKI.

To examine this, PANC1 cells were incubated with control medium or medium containing Dp44mT (10 μM), GSKI (25 μM), or both for 24 h/37 °C (Fig. 9A(*i*)). The cells were then washed, followed by an incubation for 24 h/37 °C with either control medium or medium containing either MG132 (10 μM) or Baf A1 alone (100 nM; Fig. 9A(*i*)). As shown previously (Fig. 5C), Dp44mT followed by a secondary incubation with MG132 for 24 h was able to significantly ($p < 0.01$) increase the top NDRG1 band (Fig. 9A(*ii, iii*), Lane 5) relative to Dp44mT alone (Fig. 9A(*ii, iii*), Lane 4). In cells incubated with Dp44mT and GSKI, then followed by a secondary incubation with MG132 for 24 h (Fig. 9A(*ii, iii*), Lane 11), there was a significant ($p < 0.05$) suppression in the top NDRG1 band compared to cells incubated with Dp44mT followed by MG132 alone (Fig. 9A(*ii, iii*), Lane 5). A similar suppressive effect of GSKI was also observed for p-NDRG1 (Ser330), but not for p-NDRG1 (Thr346) (Supplemental Fig. 2A; lane 5 *vs.* 11). Moreover, another well-characterized GSK3β inhibitor, LiCl (20 mM; Supplemental Fig. 3; lane 5 *vs.* 11) [59], showed similar effects as observed with the GSKI (*i.e.*, SB216763; Fig. 9A). These results are concordant with the results in Fig. 7A, where GSKI inhibited the top NDRG1 band after a 24 h incubation.

Previous studies have shown that GSK3β inhibition can promote lysosomal-dependent degradation of certain proteins [61]. Hence, the decrease in the top NDRG1 band observed in Figs. 7A, 9A, may be due to additional degradation mechanisms apart from inhibition of GSK3β

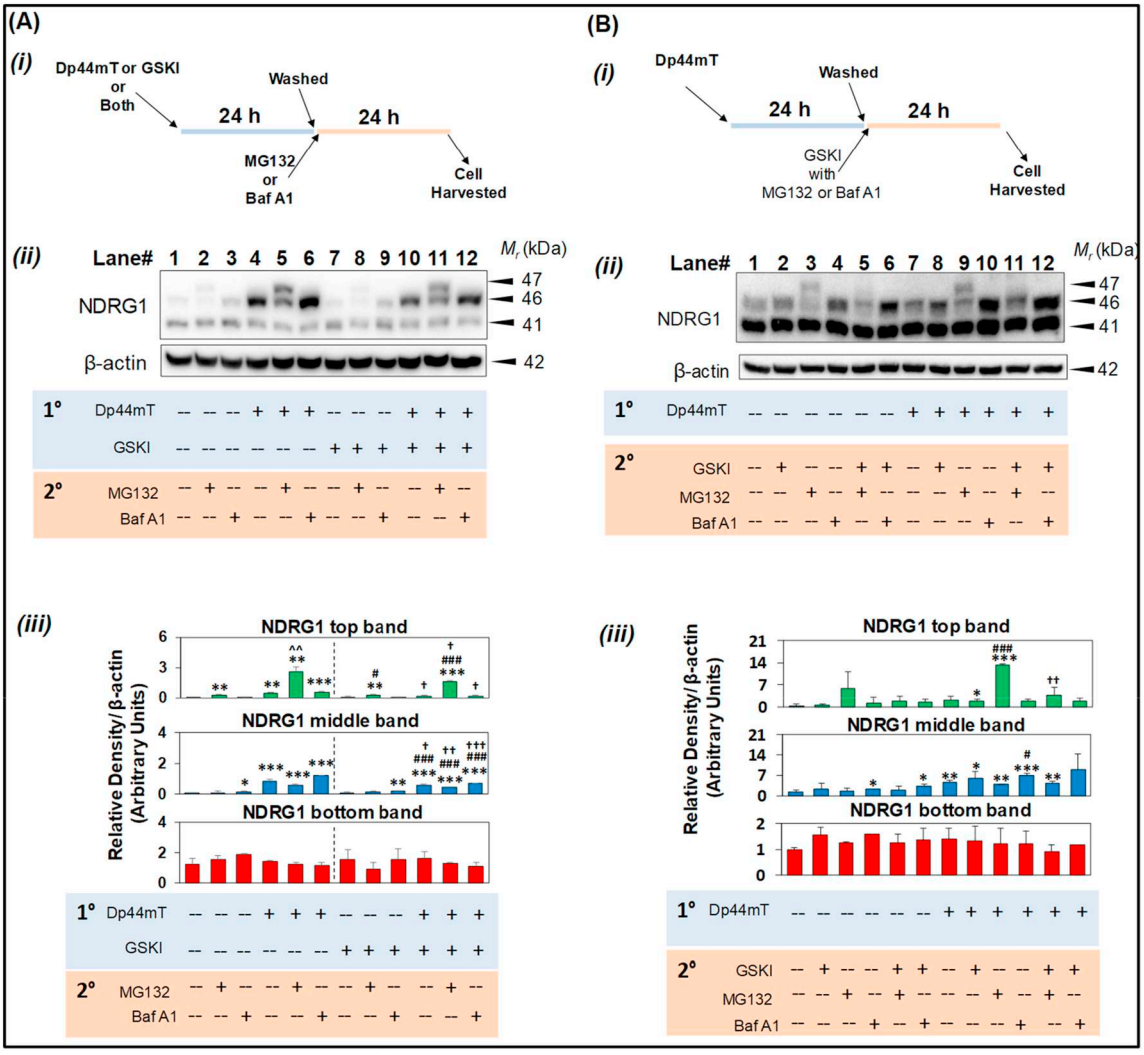

Fig. 9. Inhibition of GSK3β by the inhibitor, SB216763, results in a proteasome-independent decrease of the top NDRG1 band. A(*i*) PANC1 cells were incubated for 24 h/37 °C with or without Dp44mT (10 μM) in combination with the GSKI (25 μM). The cells were washed, followed by incubation with control medium or medium containing MG132 (10 μM) or Baf A1 (100 nM) for 24 h/37 °C. A(*ii*) Immunoblotting was then performed to investigate levels of the different NDRG1 isoforms. A(*iii*) Densitometric analysis (arbitrary units) of the results in A(*ii*). β-actin was used as a loading control. Results are shown as mean ± S.D. (3 experiments). $*p < 0.05$; $**p < 0.01$; $***p < 0.001$ compared to control cells. $\#p < 0.05$; $\#\#\#p < 0.001$ compared to GSKI alone. $\dagger p < 0.05$, $\dagger\dagger p < 0.01$; $\dagger\dagger\dagger p < 0.001$ compared to the corresponding treatments in the absence of GSKI. $\hat{}\hat{}p < 0.001$ compared to the corresponding treatments in the absence of MG132. B(*i*) PANC1 cells were incubated for 24 h/37 °C with or without Dp44mT (10 μM). The cells were then washed, followed by incubation with, control medium or medium containing GSKI (25 μM) and either MG132 (10 μM) or Baf A1 (100 nM) for 24 h/37 °C. B(*ii*) Immunoblotting was then performed to investigate levels of the different isoforms of NDRG1. B(*iii*) Densitometric analysis (arbitrary units) of results in B(*ii*). β-actin was used as a loading control. Results are shown as mean ± S.D. (3 experiments). $*p < 0.05$; $**p < 0.01$; $***p < 0.001$ compared to control cells. $\#p < 0.05$; $\#\#\#p < 0.001$ compared to Dp44mT alone. $\dagger\dagger p < 0.01$; compared to the corresponding treatments in the absence of GSKI.

kinase activity. To examine a direct role of the GSKI in the degradation of the top NDRG1 band, apart from its ability to inhibit GSK3β kinase activity, a modified treatment strategy was employed (Fig. 9B(*i*)). Initially, PANC1 cells were incubated with or without Dp44mT for 24 h/37 °C (10 μM; Fig. 9B(*i*)). Then, the cells were washed, followed by incubation with GSKI (25 μM) and either MG132 (10 μM) or Baf A1 (100 nM; Fig. 9B(*i*)). There was a significant ($p < 0.001$) increase in the top NDRG1 band after primary incubation with Dp44mT followed by a secondary incubation with MG132 (Fig. 9B(*ii, iii*), Lane 9), compared to the corresponding control cells treated with Dp44mT alone (Fig. 9B(*ii, iii*), Lane 7). Notably, in the presence of GSKI and MG132 in the secondary incubation, there was a marked and significant ($p < 0.01$) reduction in the top band (Fig. 9B(*ii, iii*), Lane 11), relative to the ability of MG132 alone to increase the top NDRG1 (Fig. 9B(*ii, iii*), Lane 9). These results demonstrate the ability of GSKI to decrease the top NDRG1 band independently of proteasomal degradation. Similar suppressive effect of GSKI was also observed for p-NDRG1 (Ser330), but not for p-NDRG1 (Thr346) (Supplemental Fig. 2B; lane 9 *vs.* 11). Moreover, incubation of cells with another GSK3β inhibitor, LiCl (20 mM; Supplemental Fig. 4; lane 9 *vs.* 11), also resulted in similar effects on top NDRG1 band as observed for the GSKI, *i.e.*, SB216763 (Fig. 9B). This result suggests that the GSKI has decreased the top NDRG1 band either by increasing degradation by a proteasomal-independent mechanism, or increasing dephosphorylation.

3.10. SGKI is not involved in the degradation of top NDRG1 band

The next set of experiments were performed to examine the role of SGKI in degradation/processing of the top NDRG1 band that was observed in Fig. 8. Considering the involvement of both the proteasome and lysosomal pathways in NDRG1 processing/degradation (Figs. 1, 2A), studies examined the effect of proteasomal or lysosomal inhibition

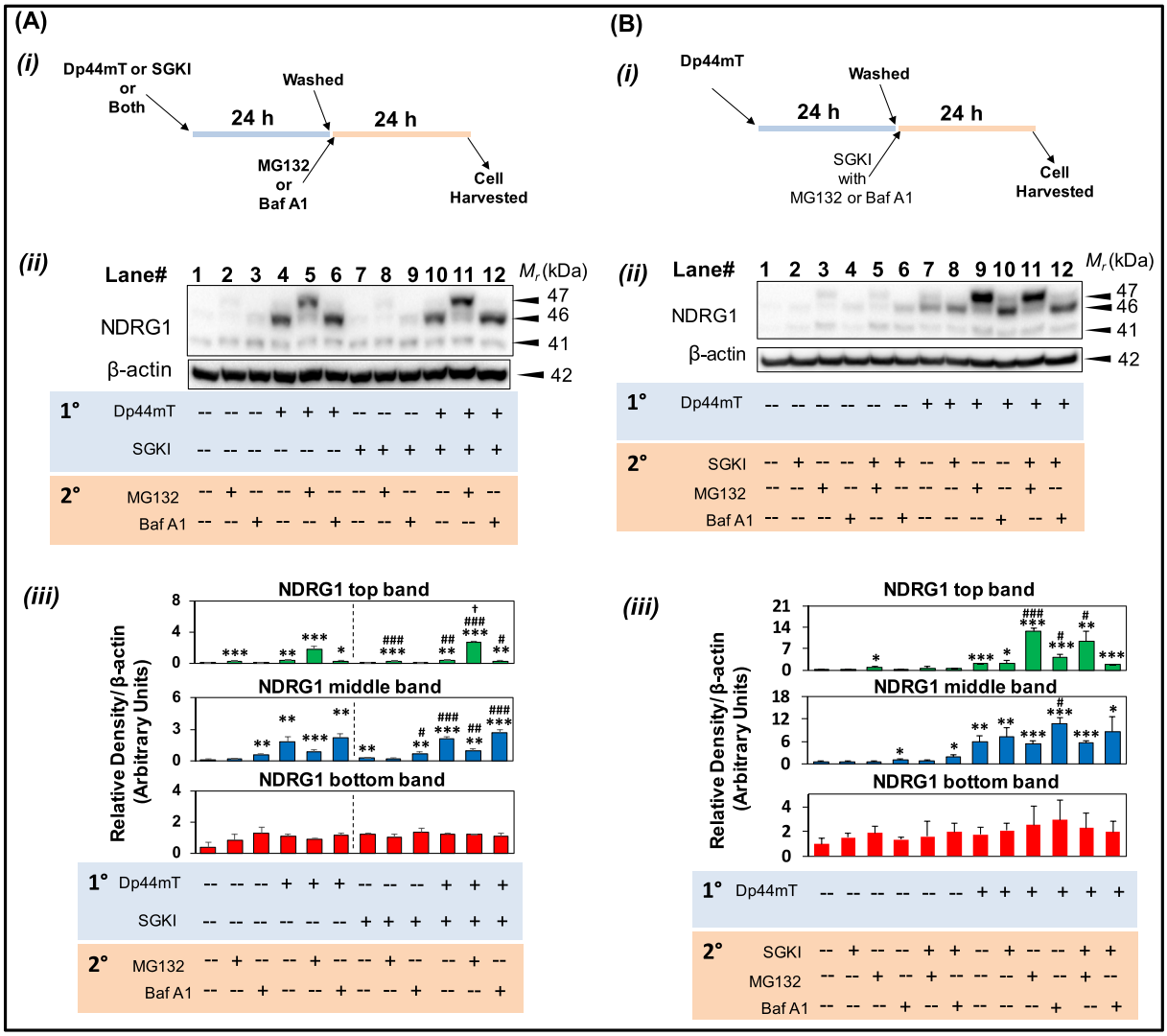

Fig. 10. SGK1 inhibition by the inhibitor GSK650394, does not affect the processing of the top NDRG1 band. A(*i*) PANC1 cells were incubated for 24 h/37 °C with either Dp44mT (10 μM) or SGKI (25 μM) or both. The cells were then washed, followed by incubation with control medium or medium containing MG132 (10 μM) or Baf A1 (100 nM) for 24 h/37 °C. A(*ii*) Immunoblotting was then performed to investigate levels of the different isoforms of NDRG1. A(*iii*) Densitometric analysis (arbitrary units) of results in A(*ii*). β-actin was used as a loading control. Results are shown as mean ± S.D. (3 experiments). *$p < 0.05$; **$p < 0.01$; ***$p < 0.001$ compared to control cells. #$p < 0.05$; ##$p < 0.01$; ###$p < 0.001$ compared to SGKI alone. †$p < 0.05$, compared to the corresponding treatments in the absence of SGKI. B(*i*) PANC1 cells were incubated for 24 h/37 °C with or without Dp44mT (10 μM). The cells were then washed, followed by incubation with control medium or medium containing SGKI (25 μM) and either MG132 (10 μM) or Baf A1 (100 nM) for 24 h/37 °C. B(*ii*) Immunoblotting was then performed to investigate levels of the different NDRG1 isoforms. B(*iii*) Densitometric analysis (arbitrary units) of results in B(*ii*). β-actin was used as a loading control. Results are shown as mean ± S.D. (3 experiments). *$p < 0.05$; **$p < 0.01$; ***$p < 0.001$ compared to control cells. #$p < 0.05$; ###$p < 0.001$ compared to Dp44mT alone.

after suppression of the top NDRG1 band by the SGKI. In initial experiments, PANC1 cells were primarily incubated with control medium or medium containing either Dp44mT (10 μM), SGKI (25 μM), or both for 24 h/37 °C (Fig. 10A(*i*)). The cells were then washed, followed by a secondary incubation with either control medium or medium containing MG132 (10 μM) or Baf A1 (100 nM) for 24 h/37 °C (Fig. 10A(*i*)).

In contrast to GSKI (Fig. 9A), in cells incubated with Dp44mT and SGKI followed by a secondary incubation with MG132 (*i.e.*, Fig. 10A(*ii*, *iii*); Lane 11), there was a significant ($p < 0.05$) increase in the top NDRG1 band compared to cells incubated with Dp44mT followed by a secondary incubation with MG132 (*i.e.*, Fig. 10A(*ii*, *iii*); Lane 5). As SGKI significantly suppressed the Dp44mT-induced top-NDRG1 band in the absence of MG132 (Fig. 8A, B), the observed increase in the top NDRG1 band after secondary incubation with MG132 (Fig. 10A(*ii*, *iii*)) could be due to build-up of NDRG1 resulting from inhibition of the proteasome during the secondary incubation. A similar effect was observed with the top p-NDRG1 (Ser330) (Supplemental Fig. 5A; Lane 5 *vs.* 11), as demonstrated with the total NDRG1 band (Fig. 10A). However, there was no significant effect of SGKI on the top p-NDRG1 (Thr346) band in the presence or absence of MG132 (Supplemental Fig. 5A; Lane 5 *vs.* 11).

Further, as the GSKI was shown to affect the top NDRG1 band independent of its ability to inhibit the kinase activity of GSK3β (Fig. 9B (*i*)), further studies examined if SGKI could modulate the levels of the top NDRG1 band, in an analogous manner (Fig. 10B(*i*)). To assess this, PANC1 cells were first incubated with or without Dp44mT for 24 h/37 °C (10 μM; Fig. 10B(*i*)). Then, the cells were washed, followed by incubation with SGKI (25 μM) and either MG132 (10 μM) or Baf A1 (100 nM; Fig. 10B(*i*)). There was a significant ($p < 0.001$) increase in the top NDRG1 band after primary incubation with Dp44mT followed by a secondary incubation with MG132 (Fig. 10B(*ii*, *iii*), Lane 9), compared to the corresponding control cells treated with Dp44mT alone (Fig. 10B(*ii*, *iii*), Lane 7). Notably, in the presence of SGKI in the secondary incubation, there was no significant ($p > 0.05$) reduction in

the ability of MG132 to increase the top NDRG1 (Fig. 10B(*ii*, *iii*), Lane 11), compared to corresponding treatments with MG132 alone (Fig. 10B(*ii*, *iii*), Lane 9). These results demonstrate that SGKI, in contrast to GSKI (Fig. 9B(*ii*, *iii*)), has no effect on the top NDRG1 band in the presence of proteasomal inhibition. Similarly, there was no effect of SGKI in the presence of MG132 on the top band of p-NDRG1 (Ser330) or p-NDRG1 (Thr346) (Supplemental Fig. 5B; Lane 9 *vs.* 11). Collectively, these results suggest that the SGKI mainly acts as a suppressor of kinase activity when incubated with Dp44mT (Fig. 8A).

4. Discussion

NDRG1 is an intriguing metastasis suppressor that has been demonstrated to play a role inhibiting the progression and metastasis of a variety of solid tumors, including pancreatic cancer [2]. NDRG1 has been shown to inhibit a number of critical oncogenic cellular signaling pathways (*e.g.,* EGFR pathway, ROCK-pMLC, FAK-paxillin, Src, β-catenin, *etc.*) in cancer cells [3,4,8–10,54].

Previous studies using immunoblotting have reported the presence of three different NDRG1 isoforms that could be the product of post-translational modifications, such as phosphorylation or truncation [15,18,21,28]. To understand the mechanism(s) relating to the generation of NDRG1 isoforms, the current investigation dissected the roles of two established protein processing pathways, namely that mediated by the proteasome and lysosome. Surprisingly, both these latter protein-processing machineries affected different NDRG1 isoforms (Fig. 11A). First, the levels of the top NDRG1 band (47-kDa band) were increased by two well-characterized proteasomal inhibitors, namely MG132 and Epoxomycin [47]. Each of these inhibitors have their own specific profile of inhibiting different proteolytic activities [47], nonetheless, both increased the top NDRG1 band, demonstrating the role of the proteasome in NDRG1 processing (Fig. 11A). Second, the middle NDRG1 band (46-kDa) was increased by the lysosomal acidification inhibitor, Baf A1, that inhibits both chaperone-mediated and macro-autophagy and also 3-MA that inhibits only the latter process [38]. This suggested the middle band was being processed and potentially degraded *via* the lysosome (Fig. 11A). Of note, these well-established classical inhibitors are known to affect cellular protein degradation machinery, *i.e.*, proteasomal (*e.g.*, MG132; [47]) or autophagy (*e.g.*, Baf A1; [38]), rather than transcription/translation.

In the presence of proteasomal inhibitors, lysosomal inhibitors were unable to increase the middle NDRG1 band (Fig. 2). This suggests that a sequential processing of NDRG1 occurs with the functional proteasome being required for subsequent lysosome-mediated metabolism. These effects were observed in three different cell-types, suggesting a more general mechanism. Of interest, other proteins also have been reported to be processed by coordinated proteasomal and lysosomal metabolism, such as the EGFR [62]. Such processing of NDRG1 may be critical in terms of different aspects of its biological activities. For instance, it has been demonstrated that NDRG1 plays a role in suppressing metastasis *via* inhibiting multiple oncogenic pathways and this could, at least in part, be mediated through these different isoforms.

Throughout all studies, it was of interest that despite marked alterations in the top and middle bands by either proteasomal or lysosomal inhibitors, the effect on the bottom band was not significant nor consistent. Considering this, it could be suggested that the bottom band may not be result of subsequent processing after the lysosomal step, rather it could be result of a separate mechanism that results in cleavage of the top band (Fig. 11A). Such separate processing is consistent with previous studies where cleavage was indicated to be responsible for the bottom NDRG1 band in cancer cells. In fact, this cleavage event was consistent with pseudotrypsin digestion at the *N*-terminus between residues Cys49-Gly50, potentially leading to the NDRG1 41-kDa protein [18].

The role of both the proteasomal and autophagic pathways in NDRG1 processing was further confirmed by immunofluorescence studies using confocal microscopy. However, it should be noted that the fluorescent signal obtained by confocal microscopy represents a combination of all three NDRG1 bands and it does not distinguish between the top, middle and bottom NDRG1 isoforms. There was a slight increase in co-localization of NDRG1 with proteasomal marker (PSMD9) after incubation with MG132 or Baf A1. On the other hand, there was a marked increase in co-localization of NDRG1 with PSMD9 upon incubation MG132 and Baf A1. These findings are in accordance with our proposed model of NDRG1 processing, where processing by the proteasome then proceeds to autophagic metabolism (Fig. 11A). Thus, inhibition of both processes were required to observe a marked accumulation of NDRG1 in proteasomes. There was increased co-localization of NDRG1 with LC3 stained autophagosomes after inhibition of proteasomal and/or autophagic processing, which could be due to the downstream processing role of autophagy in NDRG1 metabolism. These findings substantiate that both proteasomal and autophagic pathways are intricately involved in NDRG1 processing.

Hypoxia is a well-known, physiologically-relevant, NDRG1-inducing factor in tumor cells [24] and in the current investigation was able to increase levels of the middle NDRG1 band (Fig. 4A). Under hypoxic conditions, the proteasomal inhibitor resulted in a marked increase in the levels of the top band, with a significant decrease in the middle NDRG1 band. In terms of the development of NDRG1 as a therapeutic target, novel thiosemicarbazone-based anti-cancer agents (*e.g.*, Dp44mT) can markedly and significantly increase the top and middle bands of NDRG1, and its phosphorylation at Ser330 and Thr346, which was correlated with its anti-cancer activity [15,28,39,45]. Furthermore, the anti-metastatic effects of these agents have been reported to be dependent on NDRG1 expression [6]. In contrast to hypoxia, which only increased the middle NDRG1 band, Dp44mT up-regulated both the top and middle bands indicating differential processing by different induction stimuli.

NDRG1 is a known to be an important metastasis suppressor, which regulates plethora of cellular pathways involved in cancer progression, such as EGFR, ROCK-pMLC, FAK-paxillin, Src, β-catenin, *etc.* [3,4,8–10,54]. In future studies, it will be interesting to assess the role of the diverse investigative conditions employed in this current study (*i.e.*, proteasomal or lysosomal inhibition or both) on the downstream NDRG1 signaling.

In this investigation, rather than focusing on other possible post-translational processes (*e.g.*, SUMOlyation; [17]), we performed detailed mechanistic studies examining NDRG1 phosphorylation and upstream kinases involved in this process. The effect of proteasomal and lysosomal inhibitors on the Dp44mT-induced top and middle NDRG1 bands directly correlated with the phosphorylated forms of this protein at Ser330 and Thr346. However, while the bottom NDRG1 band at 41-kDa was also detected after probing for phosphorylated NDRG1, its levels were not directly correlated with the bottom band of total NDRG1. Collectively, these observations suggest the top and middle NDRG1 bands are predominantly the phosphorylated forms of the protein, while the bottom band could be a cleavage product, as reported previously [18]. This remains consistent with the hypothesis described above and illustrated in the Schematic in Fig. 11A.

We further demonstrated that in the presence of the proteasomal inhibitors, Dp44mT was unable to increase the levels of the top and middle NDRG1 bands, as well as is phosphorylated forms (Figs. 5A, 6A). These observations demonstrated the role of the active proteasome in the ability of Dp44mT to induce NDRG1 expression and phosphorylation. Considering this, proteasomal inhibitors could be potentially inhibiting upstream kinases of NDRG1 that could control its phosphorylation and also potentially its activation.

Previous investigations by others have reported the phosphorylation of NDRG1 can be mediated through both GSK3β and SGK1 activity [16]. Initial studies to determine their roles in NDRG1 processing demonstrated that specific inhibitors for these kinases were able to markedly reduce the level of the top NDRG1 and p-NDRG1 bands at 47-

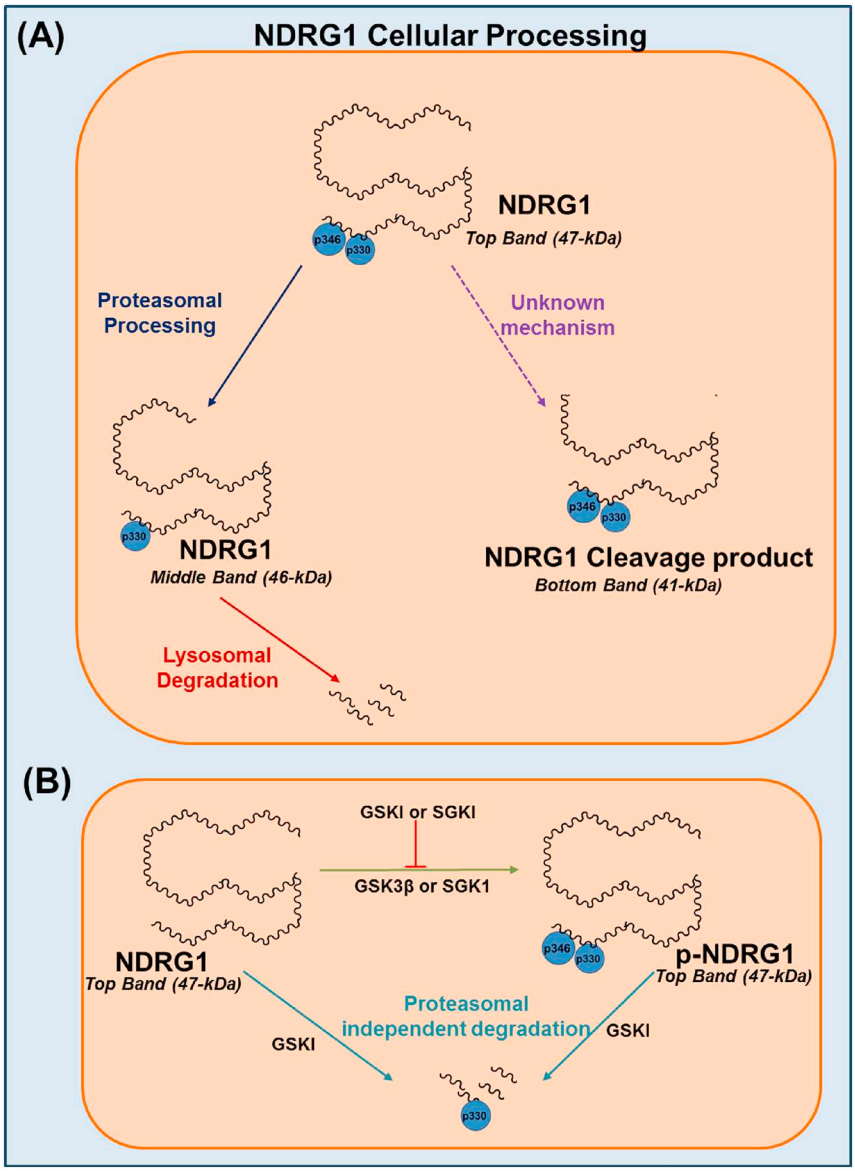

Fig. 11. Schematic diagram illustrating: (A) NDRG1 cellular processing. The various NDRG1 isoforms are the result of sequential processing by the proteasomal and lysosomal machinery (top 47-kDa and middle 46 kDa bands, respectively). Secondly, there is also a potential cleavage of NDRG1 *via* an independent, but unknown mechanism leading to the bottom 41-kDa band. The top and middle NDRG1 bands were consistently correlated to both pNDRG1 at Ser330 and Thr346. While pNDRG1 at both Ser330 and Thr346 was observed at the bottom 41-kDa band, the levels were not consistently correlated with the bottom band of total NDRG1. (B) Differential processing of NDRG1 by the upstream kinases, GSK3β and SGK1. The kinases, GSK3β and SGK1, were also shown to be involved in NDRG1 metabolism. Inhibition of GSK3β was demonstrated to decrease the levels of the top NDRG1 band, *via* a proteasomal-independent pathway. The effects of SGK1 inhibition on the top NDRG1 band were mediated by its ability to inhibit NDRG1 phosphorylation.

kDa (Figs. 7 and 8). To assess whether this observation was due to the ability of these inhibitors to decrease kinase activity, or due to alternate mechanisms, more detailed mechanistic dissection was performed. These studies demonstrated that GSK3β inhibition is involved in a kinase-independent decrease in NDRG1 levels (Fig. 11B). Previous reports have demonstrated that GSK3β inhibition can result in the activation of a lysosomal pathway [61], that could potentially be responsible for the decrease in the NDRG1 top band observed under these conditions. In contrast, the effects of SGK1 inhibition on the top NDRG1 band were demonstrated to be mediated through its ability to inhibit NDRG1 phosphorylation (Fig. 11B).

5. Conclusions

In conclusion, the multiple isoforms of NDRG1 are processed by both proteasomal and lysosomal pathways (top 47-kDa and middle 46-kDa bands, respectively) and also possibly cleavage (bottom 41-kDa band). Evidence of sequential processing of NDRG1 by the proteasome and then the lysosome was demonstrated with the top and middle bands being consistently correlated to both p-NDRG1 at Ser330 and Thr346. Furthermore, the upstream kinases, GSK3β and SGK1, were also demonstrated to be involved in the metabolism of NDRG1. For the first time, these results dissect the complex mechanisms involved in NDRG1 processing in cancer cells.

Transparency document

The Transparency document associated with this article can be found, in online version.

Acknowledgments

S.S. appreciates a Young Investigator PdCCRS Grant jointly funded by Cancer Australia and the Cure Cancer Australia Foundation. S.S. also thanks AMP Foundation for the AMP Tomorrow Fund grant. K. C. P. is a grateful recipient of Research Training Program Stipend Scholarship from the University of Sydney. ZK appreciates fellowships from the National Health and Medical Research Council of Australia and the Cancer Institute NSW as well as grant funding from the Avner Pancreatic Cancer Foundation and a PdCCRS grant jointly funded by Cancer Australia and the Cure Cancer Australia Foundation. D. R. R. appreciates a Senior Principal Research Fellowship and Project Grant funding from the National Health and Medical Research Council of Australia.

Appendix A. Supplementary data

Supplementary data to this article can be found online at https://doi.org/10.1016/j.bbadis.2019.02.008.

References

[1] Z. Kovacevic, D.R. Richardson, The metastasis suppressor, Ndrg-1: a new ally in the fight against cancer, Carcinogenesis 27 (2006) 2355–2366.

[2] B.A. Fang, Z. Kovacevic, K.C. Park, D.S. Kalinowski, P.J. Jansson, D.J. Lane, S. Sahni, D.R. Richardson, Molecular functions of the iron-regulated metastasis suppressor, NDRG1, and its potential as a molecular target for cancer therapy, Biochim. Biophys. Acta 1845 (2014) 1–19.

[3] Z. Chen, D. Zhang, F. Yue, M. Zheng, Z. Kovacevic, D.R. Richardson, The iron chelators Dp44mT and DFO inhibit TGF-beta-induced epithelial-mesenchymal transition via up-regulation of N-Myc downstream-regulated gene 1 (NDRG1), J. Biol. Chem. 287 (2012) 17016–17028.

[4] Z. Kovacevic, S.V. Menezes, S. Sahni, D.S. Kalinowski, D.H. Bae, D.J. Lane, D.R. Richardson, The metastasis suppressor, N-MYC downstream-regulated gene-1 (NDRG1), down-regulates the ErbB family of receptors to inhibit downstream oncogenic signaling pathways, J. Biol. Chem. 291 (2016) 1029–1052.

[5] J.R. Hickok, S. Sahni, Y. Mikhed, M.G. Bonini, D.D. Thomas, Nitric oxide suppresses tumor cell migration through N-Myc downstream-regulated gene-1 (NDRG1) expression: role of chelatable iron, J. Biol. Chem. 286 (2011) 41413–41424.

[6] W. Liu, F. Xing, M. Iiizumi-Gairani, H. Okuda, M. Watabe, S.K. Pai, P.R. Pandey, S. Hirota, A. Kobayashi, Y.Y. Mo, K. Fukuda, Y. Li, K. Watabe, N-myc downstream regulated gene 1 modulates Wnt-beta-catenin signalling and pleiotropically suppresses metastasis, EMBO Mol. Med. 4 (2012) 93–108.

[7] S. Bandyopadhyay, S.K. Pai, S.C. Gross, S. Hirota, S. Hosobe, K. Miura, K. Saito, T. Commes, S. Hayashi, M. Watabe, K. Watabe, The Drg-1 gene suppresses tumor metastasis in prostate cancer, Cancer Res. 63 (2003) 1731–1736.

[8] J. Sun, D. Zhang, Y. Zheng, Q. Zhao, M. Zheng, Z. Kovacevic, D.R. Richardson, Targeting the metastasis suppressor, NDRG1, using novel iron chelators: regulation of stress fiber-mediated tumor cell migration via modulation of the ROCK1/pMLC2 signaling pathway, Mol. Pharmacol. 83 (2013) 454–469.

[9] X. Wangpu, J. Lu, R. Xi, F. Yue, S. Sahni, K.C. Park, S. Menezes, M.L. Huang, M. Zheng, Z. Kovacevic, D.R. Richardson, Targeting the metastasis suppressor, N-myc downstream regulated gene-1, with novel di-2-pyridylketone thiosemicarbazones: suppression of tumor cell migration and cell-collagen adhesion by inhibiting focal adhesion kinase/paxillin signaling, Mol. Pharmacol. 89 (2016) 521–540.

[10] W. Liu, F. Yue, M. Zheng, A. Merlot, D.H. Bae, M. Huang, D. Lane, P. Jansson, G.Y. Lui, V. Richardson, S. Sahni, D. Kalinowski, Z. Kovacevic, D.R. Richardson, The proto-oncogene c-Src and its downstream signaling pathways are inhibited by the metastasis suppressor, NDRG1, Oncotarget 6 (2015) 8851–8874.

[11] S.K. Kurdistani, P. Arizti, C.L. Reimer, M.M. Sugrue, S.A. Aaronson, S.W. Lee, Inhibition of tumor cell growth by RTP/rit42 and its responsiveness to p53 and DNA damage, Cancer Res. 58 (1998) 4439–4444.

[12] K. Kokame, H. Kato, T. Miyata, Homocysteine-respondent genes in vascular endothelial cells identified by differential display analysis. GRP78/BiP and novel genes, J. Biol. Chem. 271 (1996) 29659–29665.

[13] N. van Belzen, W.N. Dinjens, M.P. Diesveld, N.A. Groen, A.C. van der Made, Y. Nozawa, R. Vlietstra, J. Trapman, F.T. Bosman, A novel gene which is up-regulated during colon epithelial cell differentiation and down-regulated in colorectal neoplasms, Lab. Investig. 77 (1997) 85–92.

[14] X. Qu, Y. Zhai, H. Wei, C. Zhang, G. Xing, Y. Yu, F. He, Characterization and expression of three novel differentiation-related genes belong to the human NDRG gene family, Mol. Cell. Biochem. 229 (2002) 35–44.

[15] K.C. Park, S.V. Menezes, D.S. Kalinowski, S. Sahni, P.J. Jansson, Z. Kovacevic, D.R. Richardson, Identification of differential phosphorylation and sub-cellular localization of the metastasis suppressor, NDRG1, Biochim. Biophys. Acta 1864 (2018) 2644–2663.

[16] J.T. Murray, D.G. Campbell, N. Morrice, G.C. Auld, N. Shpiro, R. Marquez, M. Peggie, J. Bain, G.B. Bloomberg, F. Grahammer, F. Lang, P. Wulff, D. Kuhl, P. Cohen, Exploitation of KESTREL to identify NDRG family members as physiological substrates for SGK1 and GSK3, Biochem. J. 384 (2004) 477–488.

[17] J.E. Lee, J.H. Kim, SUMO modification regulates the protein stability of NDRG1, Biochem. Biophys. Res. Commun. 459 (2015) 161–165.

[18] M.K. Ghalayini, Q. Dong, D.R. Richardson, S.J. Assinder, Proteolytic cleavage and truncation of NDRG1 in human prostate cancer cells, but not normal prostate epithelial cells, Biosci. Rep. 33 (2013) (pii: e00042).

[19] Y.M. Oh, H.B. Park, J.H. Shin, J.E. Lee, H.Y. Park, D.H. Kho, J.S. Lee, H. Choi, T. Okuda, K. Kokame, T. Miyata, I.H. Kim, S.H. Lee, R.H. Schwartz, K. Choi, Ndrg1 is a T-cell clonal anergy factor negatively regulated by CD28 costimulation and interleukin-2, Nat. Commun. 6 (2015) 8698.

[20] J.A. Gasser, H. Inuzuka, A.W. Lau, W. Wei, R. Beroukhim, A. Toker, SGK3 mediates INPP4B-dependent PI3K signaling in breast cancer, Mol. Cell 56 (2014) 595–607.

[21] Y. Murakami, F. Hosoi, H. Izumi, Y. Maruyama, H. Ureshino, K. Watari, K. Kohno, M. Kuwano, M. Ono, Identification of sites subjected to serine/threonine phosphorylation by SGK1 affecting N-myc downstream-regulated gene 1 (NDRG1)/Cap43-dependent suppression of angiogenic CXC chemokine expression in human pancreatic cancer cells, Biochem. Biophys. Res. Commun. 396 (2010) 376–381.

[22] N.T. Le, D.R. Richardson, Iron chelators with high antiproliferative activity up-regulate the expression of a growth inhibitory and metastasis suppressor gene: a link between iron metabolism and proliferation, Blood 104 (2004) 2967–2975.

[23] D.J. Lane, F. Saletta, Y. Suryo Rahmanto, Z. Kovacevic, D.R. Richardson, N-myc downstream regulated 1 (NDRG1) is regulated by eukaryotic initiation factor 3a (eIF3a) during cellular stress caused by iron depletion, PLoS One 8 (2013) e57273.

[24] H. Cangul, Hypoxia upregulates the expression of the NDRG1 gene leading to its overexpression in various human cancers, BMC Genet. 5 (2004) 27.

[25] D. Hanahan, R.A. Weinberg, Hallmarks of cancer: the next generation, Cell 144 (2011) 646–674.

[26] J. Yuan, D.B. Lovejoy, D.R. Richardson, Novel di-2-pyridyl-derived iron chelators with marked and selective antitumor activity: in vitro and in vivo assessment, Blood 104 (2004) 1450–1458.

[27] M. Whitnall, J. Howard, P. Ponka, D.R. Richardson, A class of iron chelators with a wide spectrum of potent antitumor activity that overcomes resistance to chemotherapeutics, Proc. Natl. Acad. Sci. U. S. A. 103 (2006) 14901–14906.

[28] Z. Kovacevic, S. Chikhani, D.B. Lovejoy, D.R. Richardson, Novel thiosemicarbazone iron chelators induce up-regulation and phosphorylation of the metastasis suppressor N-myc down-stream regulated gene 1: a new strategy for the treatment of pancreatic cancer, Mol. Pharmacol. 80 (2011) 598–609.

[29] D.B. Lovejoy, D.M. Sharp, N. Seebacher, P. Obeidy, T. Prichard, C. Stefani, M.T. Basha, P.C. Sharpe, P.J. Jansson, D.S. Kalinowski, P.V. Bernhardt, D.R. Richardson, Novel second-generation di-2-pyridylketone thiosemicarbazones show synergism with standard chemotherapeutics and demonstrate potent activity against lung cancer xenografts after oral and intravenous administration in vivo, J. Med. Chem. 55 (2012) 7230–7244.

[30] P. Li, X. Zheng, K. Shou, Y. Niu, C. Jian, Y. Zhao, W. Yi, X. Hu, A. Yu, The iron chelator Dp44mT suppresses osteosarcoma's proliferation, invasion and migration: in vitro and in vivo, Am. J. Transl. Res. 8 (2016) 5370–5385.

[31] H. Petra, P. Veronika, E. Éva, K. Bernhard, S. Gergely, K. Christian, Anticancer thiosemicarbazones: chemical properties, interaction with iron metabolism, and resistance development, Antioxid. Redox Signal. 30 (8) (2019) 1062–1082, https://doi.org/10.1089/ars.2017.7487.

[32] A.M. Merlot, D.S. Kalinowski, Z. Kovacevic, P.J. Jansson, S. Sahni, M.L. Huang, D.L. Lane, H. Lok, D.R. Richardson, Exploiting Cancer metal metabolism using anticancer metal-binding agents, Curr. Med. Chem. 25 (2018) 1–22.

[33] S.V. Menezes, L. Fouani, M.L.H. Huang, B. Geleta, S. Maleki, A. Richardson, D.R. Richardson, Z. Kovacevic, The metastasis suppressor, NDRG1, attenuates oncogenic TGF-beta and NF-kB signaling to enhance membrane E-cadherin expression in pancreatic cancer cells, Carcinogenesis (2018), https://doi.org/10.1093/carcin/bgy178.

[34] P.J. Jansson, D.S. Kalinowski, D.J. Lane, Z. Kovacevic, N.A. Seebacher, L. Fouani, S. Sahni, A.M. Merlot, D.R. Richardson, The renaissance of polypharmacology in the development of anti-cancer therapeutics: inhibition of the "triad of death" in cancer by di-2-pyridylketone thiosemicarbazones, Pharmacol. Res. 100 (2015) 255–260.

[35] H. Jung, S.Y. Wang, I.W. Yang, D.W. Hsueh, W.J. Yang, T.H. Wang, H.S. Wang, Detection and treatment of mycoplasma contamination in cultured cells, Chang Gung Med. J. 26 (2003) 250–258.

[36] D.R. Richardson, P.C. Sharpe, D.B. Lovejoy, D. Senaratne, D.S. Kalinowski, M. Islam, P.V. Bernhardt, Dipyridyl thiosemicarbazone chelators with potent and selective antitumor activity form iron complexes with redox activity, J. Med. Chem. 49 (2006) 6510–6521.

[37] H. Wang, X. Song, C. Logsdon, G. Zhou, D.B. Evans, J.L. Abbruzzese, S.R. Hamilton, T.-H. Tan, H. Wang, Proteasome-mediated degradation and functions of hematopoietic progenitor kinase 1 in pancreatic cancer, Cancer Res. 69 (2009) 1063–1070.

[38] D.J. Klionsky, K. Abdelmohsen, A. Abe, J. Abedin, H. Abeliovich, A. Acevedo-Arozena, C.M. Adams, P.D. Adams, K. Adeli, P.J. Adhihetty, S.G. Adler, G. Agam, R. Agarwal, M. Aghi, M. Agnello, Guidelines for the use and interpretation of assays for monitoring autophagy (3rd edition), Autophagy 12 (2016) 1–222.

[39] S. Sahni, D.H. Bae, D.J. Lane, Z. Kovacevic, D.S. Kalinowski, P.J. Jansson, D.R. Richardson, The metastasis suppressor, N-myc downstream-regulated gene 1 (NDRG1), inhibits stress-induced autophagy in cancer cells, J. Biol. Chem. 289 (2014) 9692–9709.

[40] S. Maertin, J.M. Elperin, E. Lotshaw, M. Sendler, S.D. Speakman, K. Takakura, B.M. Reicher, O.A. Mareninova, P.J. Grippo, J. Mayerle, M.M. Lerch, A.S. Gukovskaya, Roles of autophagy and metabolism in pancreatic cancer cell adaptation to environmental challenges, Am. J. Physiol. Gastrointest. Liver Physiol. 313 (2017) G524–g536.

[41] S. Krishan, D.R. Richardson, S. Sahni, The anticancer agent, di-2-pyridylketone 4,4-dimethyl-3-thiosemicarbazone (Dp44mT), up-regulates the AMPK-dependent energy homeostasis pathway in cancer cells, Biochim. Biophys. Acta 1863 (2016) 2916–2933.

[42] H. Caohuy, Q. Yang, Y. Eudy, T.A. Ha, A.E. Xu, M. Glover, R.A. Frizzell, C. Jozwik, H.B. Pollard, Activation of 3-phosphoinositide-dependent kinase 1 (PDK1) and serum- and glucocorticoid-induced protein kinase 1 (SGK1) by short-chain sphingolipid C4-ceramide rescues the trafficking defect of DeltaF508-cystic fibrosis transmembrane conductance regulator (DeltaF508-CFTR), J. Biol. Chem. 289 (2014) 35953–35968.

[43] M. Razmara, A. Monazzam, B. Skogseid, Reduced menin expression impairs rapamycin effects as evidenced by an increase in mTORC2 signaling and cell migration, Cell Commun. Signal 16 (2018) 64.

[44] J. Voelkl, T.T. Luong, R. Tuffaha, K. Musculus, T. Auer, X. Lian, C. Daniel, D. Zickler, B. Boehme, M. Sacherer, B. Metzler, D. Kuhl, M. Gollasch, K. Amann, D.N. Muller, B. Pieske, F. Lang, I. Alesutan, SGK1 induces vascular smooth muscle cell calcification through NF-kappaB signaling, J. Clin. Invest. 128 (2018) 3024–3040.

[45] Z. Kovacevic, S. Chikhani, G.Y. Lui, S. Sivagurunathan, D.R. Richardson, The iron-regulated metastasis suppressor NDRG1 targets NEDD4L, PTEN, and SMAD4 and inhibits the PI3K and Ras signaling pathways, Antioxid. Redox Signal. 18 (2013)

874–887.
[46] A. Petiot, E. Ogier-Denis, E.F. Blommaart, A.J. Meijer, P. Codogno, Distinct classes of phosphatidylinositol 3′-kinases are involved in signaling pathways that control macroautophagy in HT-29 cells, J. Biol. Chem. 275 (2000) 992–998.
[47] A.F. Kisselev, A.L. Goldberg, Proteasome inhibitors: from research tools to drug candidates, Chem. Biol. 8 (2001) 739–758.
[48] N. Mizushima, T. Yoshimori, B. Levine, Methods in mammalian autophagy research, Cell 140 (2010) 313–326.
[49] K.T. Bush, A.L. Goldberg, S.K. Nigam, Proteasome inhibition leads to a heat-shock response, induction of endoplasmic reticulum chaperones, and thermotolerance, J. Biol. Chem. 272 (1997) 9086–9092.
[50] T. Tsubokawa, I. Solaroglu, H. Yatsushige, J. Cahill, K. Yata, J.H. Zhang, Cathepsin and calpain inhibitor E64d attenuates matrix metalloproteinase-9 activity after focal cerebral ischemia in rats, Stroke 37 (2006) 1888–1894.
[51] G. Cen, K. Zhang, J. Cao, Z. Qiu, Downregulation of the N-myc downstream regulated gene 1 is related to enhanced proliferation, invasion and migration of pancreatic cancer, Oncol. Rep. 37 (2017) 1189–1195.
[52] F.E. Langlands, D. Dodwell, A.M. Hanby, K. Horgan, R.A. Millican-Slater, V. Speirs, E.T. Verghese, L. Smith, T.A. Hughes, PSMD9 expression predicts radiotherapy response in breast cancer, Mol. Cancer 13 (2014) 73.
[53] C. Rorsman, M. Tsioumpekou, C.H. Heldin, J. Lennartsson, The ubiquitin ligases c-Cbl and Cbl-b negatively regulate platelet-derived growth factor (PDGF) BB-induced chemotaxis by affecting PDGF receptor beta (PDGFRbeta) internalization and signaling, J. Biol. Chem. 291 (2016) 11608–11618.
[54] R. Jin, W. Liu, S. Menezes, F. Yue, M. Zheng, Z. Kovacevic, D.R. Richardson, The metastasis suppressor NDRG1 modulates the phosphorylation and nuclear translocation of β-catenin through mechanisms involving FRAT1 and PAK4, J. Cell Sci. 127 (2014) 3116–3130.
[55] L.E. Huang, J. Gu, M. Schau, H.F. Bunn, Regulation of hypoxia-inducible factor 1alpha is mediated by an O2-dependent degradation domain via the ubiquitin-proteasome pathway, Proc. Natl. Acad. Sci. U. S. A. 95 (1998) 7987–7992.
[56] B. Patel, A.M. Cuervo, Methods to study chaperone-mediated autophagy, Methods 75 (2015) 133–140.
[57] M.E. Hubbi, H. Hu, Kshitiz, I. Ahmed, A. Levchenko, G.L. Semenza, Chaperone-mediated autophagy targets hypoxia-inducible factor-1alpha (HIF-1alpha) for lysosomal degradation, J. Biol. Chem. 288 (2013) 10703–10714.
[58] Z. Kovacevic, D. Fu, D.R. Richardson, The iron-regulated metastasis suppressor, Ndrg-1: identification of novel molecular targets, Biochim. Biophys. Acta 1783 (2008) 1981–1992.
[59] P. Cohen, M. Goedert, GSK3 inhibitors: development and therapeutic potential, Nat. Rev. Drug Discov. 3 (2004) 479.
[60] A.B. Sherk, D.E. Frigo, C.G. Schnackenberg, J.D. Bray, N.J. Laping, W. Trizna, M. Hammond, J.R. Patterson, S.K. Thompson, D. Kazmin, Development of a small-molecule serum-and glucocorticoid-regulated kinase-1 antagonist and its evaluation as a prostate cancer therapeutic, Cancer Res. 68 (2008) 7475–7483.
[61] N. Zhang, X. Liu, L. Liu, Z. Deng, Q. Zeng, W. Pang, Y. Liu, D. Song, H. Deng, Glycogen synthase kinase-3β inhibition promotes lysosome-dependent degradation of c-FLIPL in hepatocellular carcinoma, Cell Death Dis. 9 (2018) 230.
[62] K.E. Longva, F.D. Blystad, E. Stang, A.M. Larsen, L.E. Johannessen, I.H. Madshus, Ubiquitination and proteasomal activity is required for transport of the EGF receptor to inner membranes of multivesicular bodies, J. Cell Biol. 156 (2002) 843–854.